Thin Film Processing of Photorefractive $BaTiO_3$

NASA Research Grant NAG-1-1247

Annual progress report to

Dr. Sharon Welch
NASA Langley Research Center
Hampton, Virginia 23665

Principal Investigator: Dr. Paul R. Schuster
(301) 953-6239

January 1993

Milton S. Eisenhower Research Center
Applied Physics Laboratory
The Johns Hopkins University
Laurel, MD 20723-6099

Thin Film Processing of Photorefractive $BaTiO_3$

NASA Research Grant NAG-1-1247

Annual progress report to

Dr. Sharon Welch
NASA Langley Research Center
Hampton, Virginia 23665

Principal Investigator: Dr. Paul R. Schuster
(301) 953-6239

January 1993

Milton S. Eisenhower Research Center
Applied Physics Laboratory
The Johns Hopkins University
Laurel, MD 20723-6099

TABLE OF CONTENTS

TABLE OF ILLUSTRATIONS

I. OBJECTIVES:

The principle objectives of this ongoing research project involve the synthesis, evaluation, and characterization of high optical quality films of $BaTiO_3$, which demonstrate a photorefractive response.

II. SUMMARY:

During the period covered by this report, October 11^{th}, 1991 through October 10^{th}, 1992, the research has progressed in a number of different areas. The sol-gel technique was initially studied and experimentally evaluated for depositing films of $BaTiO_3$. The difficulties with the precursors and the poor quality of the films deposited lead to the investigation of pulsed laser deposition as an alternative approach. The development of the pulsed laser deposition technique has resulted in continuous improvements to the quality of deposited films of $BaTiO_3$. The initial depositions of $BaTiO_3$ resulted in amorphous films, however, as the pulsed laser deposition technique continued to evolve, films were deposited in the polycrystalline state, then the textured polycrystalline state, and most recently heteroepitaxial films have also been successfully deposited on cubic (100) oriented $SrTiO_3$ substrates.

A novel technique for poling samples at room temperature and in air is also undergoing development with some very preliminary but positive results. The analytical techniques, which include x-ray diffraction, ferroelectric

analysis, UV-Vis spectrophotometry, scanning electron microscopy with x-ray compositional analysis, optical and polarized light microscopy, and surface profilometry have been enhanced to allow for more detailed evaluation of the samples. In the area of optical characterization, a pulsed Nd:YAG laser has been incorporated into the experimental configuration. Now data can also be acquired within various temporal domains resulting in more detailed information on the optical response of the samples and on their photorefractive sensitivity.

The recent establishment of collaborative efforts with two departments at The Johns Hopkins University and the Army Research Lab at Fort Belvoir has also produced preliminary results using the metallo-organic decomposition technique as an alternative method for thin film processing of $BaTiO_3$. RF and DC sputtering is another film deposition approach that should be initiated in the near future. Other techniques for optical characterization, which may even allow for intragranular (within single grains) investigations, are also being considered. END

III. MATERIALS PREPARATION:

METALLO-ORGANIC DECOMPOSITION (MOD):

The two methods originally proposed for preparation of the $BaTiO_3$ films were sputtering and sol-gel processing. After extensive study, it has been determined that the metallo-organic decomposition technique (MOD) is a more

efficient technique than sol-gel and it offers greater versatility. Also the problems associated with the sol-gel method (as discussed in last year's report), such as precipitate formation and incompatible hydrolysis rates of the metal alkoxides, do not occur with the metallo-organic technique. The sol-gel technique has been successful in the preparation of polycrystalline ferroelectric films of $BaTiO_3$ (Fig. 1). However, these films have been of poor optical quality and many were contaminated by the formation of a precipitate within the grains. Therefore, efforts are now being concentrated on the MOD technique in place of the sol-gel process.

Metallo-organic decomposition is a technique in which the precursors are dissolved and mixed in an appropriate solvent to form a solution (Fig. 2). The solution may be deposited onto a substrate in a variety of ways, but spin coating and dip coating are the two approaches of interest for this project. Pyrolysis is then utilized in order to drive off the remaining organics. Other steps, such as pre-baking and annealing, can also be incorporated into the process. Another advantage of this technique is that it does not require a vacuum, therefore, it can be performed in either air or some other suitable environment. Single crystal substrates, including $LaAlO_3$, MgO, LiF, and $SrTiO_3$, with a (100) orientation and a lattice mismatch less than 7% are being utilized.

SPUTTERING RELATED PROCESSES:

Pulsed-laser Ablation/Deposition (PLD):

Pulsed laser deposition has undergone the most extensive investigation over the past year. Deposition has been accomplished through the use of both an excimer laser (λ=193 nm) and for "proof of concept" a Nd:YAG laser (λ=1064 nm). Initial depositions, using the Nd:YAG laser, took place in air. The target material was a small piece of single crystal $BaTiO_3$, which was neither poled nor polished. The substrates were borosilicate glass and single crystal silicon (111). When viewed under an optical microscope, the deposited material appeared as grey ash and was composed of microcrystallites. The following depositions took place in a weak vacuum (millitorr range) within a portable vacuum chamber. Films were deposited on both silicon and fused silica substrates. Surface profilometry studies indicated film thicknesses of 1.5 to 3 microns. Optical and ferroelectric measurements on these samples demonstrated minimal response.

The films were heat treated in flowing oxygen. The heating cycle went from 25°C to 750°C in two hours and then the films were held at 750°C for 10 hours and finally cooled back down from 750°C to room temperature over a 9 hour period. Poling was also attempted by bringing the films to a temperature of 150°C (above the Curie temp. at 132°C) while applying 1.5 kV across the samples. The optical and electrical measurements showed no dramatic changes.

A number of films were deposited and evaluated. Two representative photomicrographs from an optical microscope at about 50x show the condition of the film both before and after heat treatment in an oxygen-rich environment (Figs. 3,4). The x-ray diffraction pattern does indicate crystallinity (Fig. 5), but the grains are randomly oriented similar to powder samples.

Using the Nd:YAG laser with the portable vacuum chamber did not allow for the control of certain critical parameters, which include the temperature of the substrate and the oxygen pressure during deposition and cooling. Since absorption does play a major part in the success of this technique, the wavelength of the incident radiation is also critical. As stated by Cheung and Horwitz [1], when IR radiation is used an equilibrium type of thermal heating may take place at the target. If a strictly thermal process does take place, the differences in the equilibrium vapor pressures of those components which make up the target will directly influence the composition of the plume, resulting in changes to the stoichiometry of the deposited film.

For depositing oxide thin films using pulsed laser deposition, UV radiation provides a number of advantages. The absorbed energy causes rapid nonequilibrium heating, which results in melting and vaporization of material at the target surface [2]. The vaporization pressure ejects the heated material from the target surface in both liquid and vapor forms. This plasma that is generated will attenuate,

to some extent, the energy remaining in the incident pulse. For IR radiation, this attenuation can be significant, thereby, diminishing the deposition rate. To eliminate a number of these problems, an excimer laser with a fully developed vacuum system and a substrate heater were utilized (Fig. 6). Using the UV radiation, the technique can be summarized as follows:

1) short intense pulses of coherent radiation impinge on a target,

2) photons are absorbed by the target surface causing heat to be generated within the material,

3) the material at the surface melts and then vaporizes,

4) the vaporization pressure acts as a recoil pressure and causes molten material to be ejected from the target surface forming a plume,

5) the plume is composed of material in both liquid and vapor phases which is re-deposited onto a heated substrate (Fig. 7). A one-dimensional steady-state model describing the interaction of the incident radiation with the target material is presented by Chan and Mazumder [2].

Optimizing the deposition parameters does involve the analysis and characterization of a large number of deposited films. Some of the parameters which must be controlled include the following:

1) oxygen pressure during deposition and cooling.
2) temperature of the substrate during deposition.
3) uniformity of heating across the deposition area.
4) cooling rate as dictated by the differences in the coefficients of thermal expansion/contraction between the film material and the substrate material.

$BaTiO_3$ linear coefficient varies as it goes through phase transitions: ranges from approx. 4 to 6 x 10^{-6}/°C.
5) lattice mismatch between the substrate and the film. $BaTiO_3$ lattice parameters: a=b=3.992 Å and c=4.036 Å.
6) crystallographic structure and orientation of the substrate (preferably (100)).
7) target (plume) condition and location with respect to the substrate.

The temperature feed-back system is composed of an optical pyrometer connected to a temperature controller. This system is operational from 250°C to 1050°C, however, manual control must be utilized within the temperature range of 25°C - 250°C. The system was calibrated using temperature indicating liquids (Omegalaq) with an accuracy of ±1%.

Laser fluence and the distance between the target and substrate are parameters which have a tremendous influence on the deposition rate. Davis and Gower state that at a laser fluence of 1.5 to 2 J/cm^2, the film deposition rate begins to reach a plateau at 0.2 to 0.25 Å/pulse. This range in the incident fluence was maintained by adjusting the input laser energy at a constant laser beam spot size of about 6 x 10^{-2} cm^2. In order to maximize deposition rate, the target to substrate distance was also adjusted throughout the film processing. The substrate is normally situated just beyond the terminus of the plume. In this way, a large portion of the material ablated from the target will be directed onto the substrate without adversely affecting the material (film) previously deposited.

The procedures and deposition parameters for representative films are presented in Table I. The list

is not meant to be exhaustive, but indicates many of the different approaches used in an attempt to deposit high quality films of $BaTiO_3$. Results from representative films on various substrates will be discussed in the "Results and Discussion Section". After an extensive literature study of various substrate materials, it was determined that single crystal $SrTiO_3$ with a (100) orientation would be the optimal choice. There were, however, other materials such as lithium fluoride, lanthanum aluminate, and magnesium oxide which did show potential for use as substrates in the deposition of $BaTiO_3$ films. Also, many of these substrates were, in fact, readily available within the Laboratory in the desired form ((100) orientation and polished). Therefore depositions were attempted on a number of different substrates, in an effort to determine the optimum parameters for heteroepitaxial growth of $BaTiO_3$ films.

BARIUM TITANATE ON FUSED SILICA: $BaTiO_3$ on SiO_2:

The fused silica substrates are amorphous with very low thermal expansion. These substrates were useful in the design and initial construction of the deposition system. However, because of their noncrystalline structure, they were not the substrate of choice for depositing high optical quality single crystal films of $BaTiO_3$.

BARIUM TITANATE ON SILICON: $BaTiO_3$ on Si:

The silicon substrates are semiconducting single crystals with a diamond-like cubic structure at room temperature and a (111) orientation. The lattice constant is 5.43 Å, which

results in a rather large lattice mismatch with both the a- and c-axes of tetragonal $BaTiO_3$ (mismatch of 36% with the a-axis and 34.5% with the c-axis). These substrates are useful in the alignment of the system and especially in the ferroelectric characterization of the thin films.

BARIUM TITANATE ON LITHIUM FLUORIDE: $BaTiO_3$ on LiF:

The lithium fluoride substrates are single crystals with a cubic crystalline structure at room temperature and a (100) orientation, as indicated by their x-ray pattern (Fig. 8). The lattice constant for this material is 4.027 Å, which results in a very good lattice match with tetragonal $BaTiO_3$. The lattice mismatch is only about 0.88% for the a-axis and 0.22% for the c-axis, however, lithium fluoride is a material which cleaves very easily. It is sensitive to thermal gradients and rapid thermal changes (thermal shock). Therefore, the heating and cooling rates for this material must be minimized to avoid induced stress (both thermal and mechanical). Even when taking precautions, such as heating and cooling at a rate no greater than 1°C/min, delaminations and cleavage of the material were both readily apparent during the actual deposition process.

BARIUM TITANATE ON LANTHANUM ALUMINATE: $BaTiO_3$ on $LaAlO_3$:

The lanthanum aluminate substrates are single crystals with a slight rhombohedral distortion from a cubic crystalline structure at room temperature, as indicated by their x-ray pattern (Fig. 9). These substrates have a (100) orientation and a lattice constant in the pure cubic phase (above 435°C)

of 3.792 Å, which results in a lattice mismatch of 5% with the a-axis and 6% with the c-axis.

BARIUM TITANATE ON MAGNESIUM OXIDE: $BaTiO_3$ on MgO:

The magnesium oxide substrates are single crystals with a cubic crystalline structure at room temperature and a (100) orientation, as indicated by their x-ray pattern (Fig. 10). The lattice constant for this material is 4.212 Å, which results in a lattice mismatch of 5.5% with the a-axis and 4.4% with the c-axis.

BARIUM TITANATE ON STRONTIUM TITANATE: $BaTiO_3$ on $SrTiO_3$:

The strontium titanate substrates are single crystals with a cubic crystalline structure (perovskite) at room temperature and a (100) orientation, as indicated by their x-ray pattern (Fig. 11). The lattice constant for this material is 3.905 Å, which results in a lattice mismatch of 2.2% for the a-axis and 3.2% for the c-axis.

As stated earlier, the condition of the target is also of importance, because it dictates the characteristics of the plume. Using the technique described by Davis and Gower, sintered pellets 1 inch in diameter were made from Aldrich 99.9% purity $BaTiO_3$ dry powder [3]. The powder was compressed into a pellet and then heated in a fused silica tube furnace. The temperature was ramped up from room temperature up to 1000°C at a rate of 400°C/hour with a slow flow of oxygen. The pressed pellet was held at 1000°C for 2 hours and then cooled down to 140°C at a rate of 200°C/hour. Cooling through the Curie temperature (about 130°C), from

140°C to 110°C, took place at a rate of 1°C/hour. Then the target was cooled down to room temperature at the natural rate of the furnace.

Initially the excimer laser was operated at an energy level of 75 mJ/pulse and a repetition rate of 10 Hz. However, the quality of the films seemed to improve when deposition took place at a higher incident fluence and a lower repetition rate. Therefore, the incident energy per pulse was increased to about 100 mJ/pulse and the laser beam spot size at the target was reduced to 4×10^{-2} cm^2 from the original 6×10^{-2} cm^2. The laser repetition rate was reduced to 5 Hz, and the laser was rastered over the target to avoid preferential wear. The initial depositions resulted in amorphous films of $BaTiO_3$, but with successive improvements to the technique, polycrystalline films, then textured polycrystalline films, and most recently heteroepitaxial films have also been deposited (see "Results and Discussion Section").

IV. ANALYTICAL TECHNIQUES:

Films processed through pulsed laser deposition require analytical investigation into areas which include the following: crystal structure and orientation, stoichiometry and microstructural analysis, optical and nonlinear optical response. X-ray diffraction provides data for determining the crystallinity of the samples and the orientation of their grains. This information is crucial, because $BaTiO_3$

exhibits photorefractivity when it is in the tetragonal form.

Depositing a film in the desired crystalline state with the correct orientation is by far the most difficult aspect of this research project. Therefore, results from the x-ray diffraction studies dictate future steps in the processing and/or characterization of the films. The x-ray diffraction approach used to characterize these films is similar to the powder diffraction technique. The incident x-ray source is held fixed at the chromium $K\alpha$ line with a wavelength of 2.29092 Å. The angle θ represents the Bragg angle for those planes which diffract the incident radiation when satisfying Bragg's Law (Fig. 12). The diffraction angle (2θ) is adjusted from 0° to 180° such that various planar orientations have an opportunity to diffract some of the incident radiation. As 2θ is varied, a specific set of lattice planes will briefly satisfy Bragg's Law and reflect the incident x-rays, exposing the film at a particular location.

The progression from randomly oriented polycrystalline films to heteroepitaxial films is revealed in the x-ray diffraction patterns of the samples. A continuous curve with uniform intensity in the diffraction pattern represents a specific set of crystal planes (Fig. 13). These planes maintain their Bragg angle with the incident radiation but exist in all possible rotational positions about the axis of the x-ray beam. If discontinuities (intensity variations)

exist within a curve (Fig. 14), these discontinuities indicate preferences with respect to particular rotational positions (preferred orientations or texture). If the curves completely disappear and are replaced by discrete spots, this is indicative of a single crystal type of growth pattern. If the spots align with the diffraction spots from a single crystal oriented substrate of different material, then a heteroepitaxial film has been successfully deposited (Fig. 15).

Scanning electron microscopy is utilized for evaluating the quality of the film (uniformity and absence of cracks) and to observe some of its single crystal growth characteristics. X-ray compositional analysis identifies certain elements which exist in each sample and can be useful as a semi-quantitative tool for stoichiometric evaluation. As stated in last year's report, a small commercially available $BaTiO_3$ single crystal was characterized as a reference standard. Characteristics of interest include the ratios of the titanium $K\alpha$ and the barium $L\alpha$ peaks, and the percentage of the titanium versus the barium oxide. Comparisons are made between the data from the reference standard and the data acquired from various deposited films.

Since $BaTiO_3$ is optically uniaxial in the tetragonal phase, polarized light microscopy is being used for the initial qualitative analysis of the film and the observation of the orthogonal domains. Domains within $BaTiO_3$ orient

themselves at both 90° and 180° (Fig. 16). Antiparallel domains (180° orientation) can not be identified by polarized light microscopy, but must be analyzed using other techniques, chemical etchants and the pyroelectric method, as described in last year's report.

Surface profilometry is used for quantitative analysis concerning film thickness and surface roughness. UV-Vis spectrophotometry generates quantitative information on the absorption characteristics of the films. Data from these studies are compared to the data acquired from a commercially available single crystal of $BaTiO_3$.

Even if crystallinity of our samples is established by x-ray diffraction, the correct crystalline structure (tetragonal phase at room temperature) must be ascertained. Since $BaTiO_3$ is ferroelectric in the tetragonal phase, a modified Sawyer-Tower circuit [4] has been built to examine the ferroelectric behavior of the samples (Fig. 17).

V. RESULTS AND DISCUSSION:

METALLO-ORGANIC DECOMPOSITION:

Thin films of $BaTiO_3$ were deposited using the MOD technique at the Night Vision and Electro-Optics Division of the Army Research Lab at Fort Belvoir, Virginia. The starting materials chosen were barium neodecanoate and titanium 2-ethylhexoxide (unable to obtain titanium neodecanoate). The procedure utilized has been described by Shaikh and Vest in a study on the formation of $BaTiO_3$

and $PbTiO_3$ from metallo-organic precursors [5].

In the first study, 48 mg (0.1 mmol) of barium neodecanoate and 56 mg (0.1 mmol) of titanium 2-ethylhexoxide were dissolved in the solvent toluene. This produced the desired molar ratio of barium to titanium, 1:1. This solution was dilute and of low viscosity, resulting in the formation of extremely thin films (100 angstroms or less) spin coated onto single crystal silicon substrates. The mottled appearance of the film gave indications of phase segregation during the deposition process. The film was then annealed at 600°C for 1 hour. Other solvents, such as mixed xylenes, were also attempted, but produced similar results.

Higher concentrations of the precursors were utilized in the next study in order to increase the viscosity of the solution, and thereby increase the thickness of the films deposited. The dissolution of 480 mg (1.0 mmol) of barium neodecanoate (close to the solubility limit) and 560 mg (1.0 mmol) of titanium 2-ethylhexoxide took place in 100 ml of mixed xylenes. Even with the increased viscosity, twenty depositions were still necessary to obtain a film thickness of a few thousand angstroms. Three other approaches worth investigating are the following: 1) heating the solutions and/or substrates, 2) using solubilizing agents to increase solubility, and 3) adding inert viscosity enhancing agents, such as ethylene glycol. Annealing was done under the same

conditions, 600°C for 1 hour, as mentioned for the previous films.

PULSED LASER DEPOSITION:

LiF Substrates:

Deposition parameters for the majority of the deposited films are contained in Table I. As discussed earlier, the initial depositions took place on single crystal silicon and amorphous fused silica. These substrates worked well for the "proof of concept" and the alignment of the system. However, the films of higher quality were deposited on oriented single crystal substrates with a lattice mismatch of less than 7%. Youden et al. state that if attempting to deposit an epitaxial film, the lattice mismatch between the film and the substrate must be less than 7% [6].

Lithium fluoride has an excellent lattice match with tetragonal $BaTiO_3$. However, its thermal and mechanical sensitivity, plus the large difference in the thermal coefficients of expansion between LiF and $BaTiO_3$, made it rather difficult to deposit continuous films. During the initial depositions, material was actually flaking off the surface. This resulted in only a small section of the film remaining after cooling (Fig. 18). Data from x-ray diffraction, UV-Vis spectrophotometry, and optical characterization verified the nonexistence of a film (Figs. 19,20).

For these initial depositions, the substrate had been placed at the terminus of the plume, which was approximately 3 cm from the target. In an attempt to reduce the thermal effects of the high temperature plume on the substrate, the distance between the two was increased at 5 mm intervals on subsequent depositions. At approximately 5.5 cm separation distance, the flaking was minimized during deposition, but the deposition rate also greatly diminished. As stated by Geohegan in a paper on pulsed laser deposition of superconducting YBCO, deposition in a reactive gas environment, such as oxygen, will result in the scatter and attenuation of the plume, along with the formation of various oxides [7]. Geohegan also states that for pulsed laser deposition, the ambient gas pressures should be minimized to insure that some of the vaporized material of interest actually makes it to the substrate. Roy et al. have demonstrated success at depositing polycrystalline films of both $SrTiO_3$ and $BaTiO_3$, using pulsed laser deposition, at the low oxygen pressure of only 10 mTorr [8,9].

The next depositions on LiF substrates were, therefore, attempted in a pure vacuum with O_2 introduced during cooling and also at reduced O_2 pressures (see Table I). During the actual deposition, the films seemed to stay intact. However, when there was no O_2 introduced during the deposition, the films crumbled into small pieces and

broke off during the cooling process (Fig. 21). When O_2 pressures in the range of 20 mTorr were utilized during the depositions, the films remained whole even through the initial phase of the cooling process. However, at approximately 500°C the film (and probably some of the substrate) cleaved entirely off the surface and rolled up at the bottom of the vacuum chamber. Any attempt to retrieve it for examination, resulted in the film's destruction.

LiF has a thermal coefficient of expansion which starts at 37 x 10^{-6}/°C in the low temperature range of 0°C to 100°C ($BaTiO_3$: 4 to 6 x 10^{-6}/°C). As stated by Davis and Gower, this large difference in the thermal coefficients of expansion between the film and substrate leads to induced stress within the system [3]. Since the LiF substrates have such a strong tendency for cleavage, this stress had to be eliminated by reducing the cooling rate dramatically. With the Eurotherm temperature controller, the lowest rate possible for cooling was 1°C/min, which was the rate utilized in the previous attempts at deposition. Therefore, a different approach was taken; cooling would occur at a rate of 1°C/min for 55°C intervals and then the sample would be held at that temperature (dwell) for 60 minutes. This procedure was repeated until a temperature outside of the controller's range was reached (see Table I). This proved to have only limited success (partial cleavage).

Other parameters were changed in attempt to deposit films on LiF, such as repetition rate of the laser and the

incident fluence, but high optical quality continuous films were still unattainable. The temperature of the substrate during the deposition was another cause for concern when depositing on LiF. The material becomes molten and emits toxic fumes at temperatures above 847°C [10]. This limited the versatility of these substrates, since, as stated by Hubler, when attempting to deposit an epitaxial film, heating the substrate provides an additional source of energy to the deposited material [11]. This thermal energy allows the atoms which make up the film to re-arrange themselves into their most thermodynamically stable positions [11]. Therefore, even though the lattice match of the cubic LiF substrates with tetragonal $BaTiO_3$ was very good, other properties of these substrates made them less desirable.

$LaAlO_3$ Substrates:

$LaAlO_3$ substrates were also investigated because of the similarities in crystalline structure (perovskite-like) and the recent reports of some success, using chemical vapor deposition, in the processing of $BaTiO_3$ films on $LaAlO_3$ [12,13]. In order to eliminate the formation of other species within the deposited film and to enhance its crystallinity, Wills et al. utilized substrate temperatures of 800°C [13]. It is, however, very difficult to operate a resistive heating element (Kanthal:iron-chromium-aluminum alloy) at high temperatures in an oxygen-rich environment for any extended period of time. A number of heater

failures took place, which required both re-designing and re-building the heating system.

Continuous films were then deposited ranging in thickness from about 0.5 to 1 micron. Those parameters stated in Table I produced the highest quality films deposited on $LaAlO_3$ (Fig. 22). The annealing phase was to minimize the occurrence of oxygen deficiencies within the films. The x-ray diffraction pattern shows discontinuous polycrystalline powder lines (Fig. 23). This is indicative of texturing within the film (preferred orientation of the grains), an improvement over previously deposited randomly oriented polycrystalline films. Heteroepitaxial films were, however, still unattainable using these deposition parameters with $LaAlO_3$ substrates.

Depositing at higher substrate temperatures would provide more energy to the system and may produce the desired growth characteristics. However, with the heater configuration used, this was in no way possible. The other concern for promoting epitaxial growth was the phase transition of $LaAlO_3$ that occurs at 435°C during the cooling of the film. Simon et al. originally stated that only a slight rhombohedral distortion of the lattice took place at the phase transition [14]. Wills et al., in a more recent study, mentions that the lattice mismatch with tetragonal $BaTiO_3$ can, in fact, go from 5% or 6% in the cubic high temperature phase to over 30% below the phase transition temperature [13].

MgO Substrates:

The properties of MgO make it a viable alternative for use as a substrate material in the deposition of $BaTiO_3$. The lattice mismatch is slightly better than that of $LaAlO_3$, and no phase transitions take place through the temperature range utilized in the film processing. Also the thermal coefficient of expansion varies from about 7 x 10^{-6}/°C to 14 x 10^{-6}/°C in going from room temperature to 800°C [15]. As stated earlier, the thermal coefficient of expansion for $BaTiO_3$ ranges from about 4 x 10^{-6}/°C to 6 x 10^{-6}/°C, on average, only about a factor of 2 difference between the film and the substrate material. This eases the constraints on sample cooling, and minimizes the degree of thermally induced stress. As with LiF and $LaAlO_3$, the desired orientation, (100), was also readily attainable with MgO ((100) cleavage plane).

Deposition parameters used for film processing on MgO are listed in Table I. Surface profilometry indicated approximately 0.7 micron thick films of $BaTiO_3$. The x-ray diffraction pattern shows preferential orientation (Fig. 24), similar to the results seen with the films previously deposited on $LaAlO_3$. These data acquired from films deposited on both $LaAlO_3$ and MgO gave a strong indication of the need for higher substrate temperatures during the deposition in order to promote epitaxial growth. With this in mind, other substrate heaters were evaluated. A boron nitride coated pyrolytic graphite resistance heating

element was the best choice for the vacuum and pulsed laser deposition system being utilized. It offered stable high temperatures (over 2000°C within a strong vacuum), durability even in oxygen-rich environments, and was operational using a standard 110 variac [16]. The contacts, where the element is exposed, were platinum coated for resistance to degradation.

Until the new heater system was in place, a furnace was used for post-deposition high temperature annealing in an oxygen-rich environment. The temperature of the film deposited on MgO was brought up to 1000°C in a 2 hour period. It was held at 1000°C for 10 hours and ramped down to room temperature over a 2 hour period. After the annealing procedure was completed, another x-ray diffraction pattern was generated. The x-ray diffraction pattern showed very little change resulting from the post-deposition heat treatment (Fig. 25).

Various parameters were adjusted for subsequent depositions on MgO. The temperature was increased by about 30°C and the O_2 pressure was increased up to about 100 mTorr. Variations in laser repetition rates were attempted in order to determine its effect on film growth. Varying the laser repetition rate in the midst of a deposition was also done (Table I). Films were relatively smooth and measured about 1 micron in thickness (Fig. 26). In general, however, the x-ray diffraction patterns showed little or no

improvement, and in certain cases, it even appeared that the grains actually became more randomly oriented (Fig. 27).

$\underline{SrTiO_3}$ Substrates:

$SrTiO_3$ exhibited the greatest similarities to $BaTiO_3$, when comparing the various substrate materials and looking at their properties overall. The crystalline structure is cubic, of the perovskite form, and the lattice mismatch with either axis of tetragonal $BaTiO_3$ is within 3.5%. The thermal coefficient of expansion remains about $9 \times 10^{-6}/°C$ within the cubic phase, and the phase transitions take place at temperatures well outside of the range of these experiments (below -100°C).

In order to gain a better understanding with respect to the influence of temperature on the film characteristics, the first three films were deposited at three different temperatures (see Table I) and then analyzed. Films deposited at the substrate temperature of 600°C showed only slight indications of any crystallinity (Fig. 28). At substrate depositions temperatures of 800°C, the first real signs of heteroepitaxial growth became apparent. Diffraction spots from the $BaTiO_3$ film appear to be aligned with the background diffraction pattern from the $SrTiO_3$ substrate (Fig. 29). Only minimal indications of a polycrystalline nature exist. The next deposition took place at a substrate temperature of 900°C. No major improvements could be seen from the x-ray diffraction pattern (Fig. 30). In fact, the film demonstrated signs of

epitaxy in the diffraction pattern, but its alignment with the substrate's orientation was not as good as that of the previously deposited film. The absorption tail identified in the UV-Vis spectrophotometric data also confirmed the existence of the $BaTiO_3$ films through comparisons with results obtained from pure single crystal $SrTiO_3$ and $BaTiO_3$ samples (Figs. 31,32). Detailed information on the optical absorption edge of $BaTiO_3$ and on infrared spectroscopy of various perovskite titanates can be found in papers by Wemple and Perry et al. respectively [17,18].

Besides the deposition temperature, another difference noted between these two samples was the mounting of the substrate to the heater assembly with thermally conductive paint. The desired approach has been to place the conductive paint around the perimeter on the backside of the substrate, and then attach it to the face plate of the heater. This allows for optical characterization of the film to take place through the center of the sample. If a reasonably good optical quality film has been deposited, the center region should still be somewhat transparent at the visible wavelengths of interest. The conductive paint is actually a silver paste, which maintains a high viscosity through the use of an organic thinner, butyl acetate. In air, the organics are very volatile, such that the paste becomes solid, creating a good conductive path within a relatively short period of time. For the film which exhibited closer aligment to the substrate orientation,

the conductive paste was more uniformly distributed throughout the back of the substrate, not just contained around the perimeter. When that substrate was mounted on the heater, it was pressed down slightly causing the paste to spread out.

To determine if the conductivity was an issue, the subsequent depositions took place on $SrTiO_3$ substrates of half the original thickness (0.5 mm from 1 mm). The x-ray diffraction pattern from the next film deposited at 900°C on the 0.5 mm thick substrate exhibited very strong preferential orientation (Fig. 33). No continuous powder lines were even discernable. It appears that thermal conductivity must also be considered. As stated earlier, temperatures are measured by an optical pyrometer. Because of the existence of the plume and the continuous changes in emissivity at the substrate surface, the pyrometer must be focused on the substrate holder and not directly on the substrate itself. If there does not exist a good thermally conductive path, the substrate will not attain those temperatures.

Data from the last few depositions on $SrTiO_3$ demonstrated a vast improvement over any of the films previously deposited. The films were beginning to strongly orient themselves and grow in an epitaxial fashion. With a little more energy supplied to the film, heteroepitaxial growth should develop. Since the boron nitride coated pyrolytic graphite heater was still not in service, other

techniques were attempted, such as in situ annealing, for providing additional energy to the films. Data indicated no improvement (Fig. 34), leading to the decision for higher deposition temperatures.

When the new heater was finally operational, a holder with a face plate had to be constructed. The next depositions took place at 1045°C to 1050°C; the upper limit of the temperature range over which the pyrometer was operable. Owing to the limited number of 0.5 mm thick substrates readily available, the first depositions at 1045°C took place on 1 mm thick $SrTiO_3$. A very weak plume was generated during the initial deposition at this temperature. The x-ray diffraction pattern showed limited and faint indications of heteroepitaxial growth, with some diffraction spots of the film aligning with those of the target (Fig. 35). The target material was removed and examined, and determined to be no longer of use. Each target is used and re-used (sometimes requiring light sanding) until, on irradiation, a strong plume can no longer be produced.

A new target pellet was pressed from the Aldrich powder, and another film was deposited on 1 mm thick $SrTiO_3$. For another study on the thermal conductivity, the silver paste was placed randomly on the back of the substrate. Photomicrographs showed preferential growth in areas which contained the conductive paste (Fig. 36). An island type of growth appears to have taken place in this film similar

to a study reported by Liou and Wu on the growth of the tetragonal superconductor $Tl_2Ba_2Ca_2Cu_3O_x$ on single crystal MgO [19]. The x-ray diffraction pattern exhibited much more pronounced signs of heteroepitaxy (Fig. 37). Also coarse discontinuous polycrystalline powder lines were readily apparent. These are indicative of large grains with some preferred orientation [20]. The d-spacings were solved for using Bragg's Law and an attempt was made to determine the corresponding planar indices (hkl) assuming tetragonal $BaTiO_3$. However, when comparing the data to that published by the Joint Committee on Powder Diffraction Standards [21], it was clear that these polycrystalline diffraction patterns were not representative of any form of $BaTiO_3$, including the high temperature hexagonal phase. The species which produced these patterns has not yet been determined, however they may have resulted from decomposition of $BaTiO_3$ or the formation of other stable compounds made up of barium, titanium, and oxygen.

The two most recent depositions took place at the maximum temperature of 1050°C on 0.5 mm thick $SrTiO_3$ substrates with a flowing O_2 pressure of 400 mTorrs and a laser rep. rate of 5 Hz (see Table I). These parameter settings were chosen as optimum through analysis of the data acquired from the previously deposited films. No problems were detected during the deposition of the first of these two samples. Photomicrographs taken at the edge of the film suggest the possible formation of a background matrix

(Fig. 38). The photomicrograph (100x magnification) taken at the center of the film reveals large and very symmetrical grains (Fig. 39). In another area, the grains are needle-like and smaller (Fig. 40). The x-ray diffraction pattern exhibited distorted diffraction spots and very faint indications of any polycrystallinity (Fig. 41). The distorted diffraction spots are very obvious, and there does appear to be evidence of more than one set of spots. The existence of multiple diffraction spots at one location on the x-ray film is not unique to this sample. However, the pattern here is much more pronounced, and it is consistent throughout the film.

In order to see if the data were reproducible, another film was deposited under the same conditions. However, with 10 minutes left in a 2 hour deposition, the heater failed catastrophically (Fig. 42), resulting in a rapid cooling of the sample. Photomicrographs show a darker film made up of smaller grains (Fig. 43). A crack in the substrate facilitated its removal, exposing a small area of the film on top (Fig. 44). The x-ray diffraction pattern was similar to the one acquired for the previous film, but somewhat more distorted (Fig. 45).

The distorted diffraction patterns from those substrates most recently used, may have resulted from either poor quality, and/or induced stress in the material due to high temperature thermal cycling and small variations in the thermal coefficient of expansion between $BaTiO_3$ and $SrTiO_3$.

Two experiments were undertaken in an attempt to verify this hypothesis. The first involved taking an uncoated 0.5 mm thick $SrTiO_3$ substrate and running it through the entire film deposition process without actually depositing a film on it. Afterwards, an x-ray diffraction patten was taken and examined. The resulting diffraction spots showed no apparent distortion (Fig. 46). This implies that the film deposition process, including the high temperature cycling, has minimal effect on an uncoated $SrTiO_3$ substrate. The second study involved randomly choosing another $SrTiO_3$ substrate and examining its "off the shelf" condition through x-ray diffraction. It can be seen in figure 47 that the quality of the substrates does, in fact, vary. Diffraction spots from this particular substrate, which had not been used in any fashion, are distorted and even show splitting in certain areas.

Initial indications of a heteroepitaxial type growth in the last two films warranted additional detailed examination. The first film was cooled under more ideal, controlled, and reproducible conditions, and was, therefore, chosen for further investigation. Ferroelectric analysis and optical studies of photorefractivity produced no significant results. Scanning electron microscopy (SEM) was then performed on this sample for analysis of its microstructure and composition. The SEM photomicrographs at 200x magnification begin to reveal grains with a specific geometric shape - hexagonal (Figs. 48,49). Some of the

grains even appear to be growing from out of the background matrix material. At a magnification of 5000x, this SEM photomicrograph displays a grain, 5 to 10 microns on an edge, with a very symmetrical hexagonal shape (Fig. 50). The contrast variations arise from induced charging (films were not sputter coated for SEM). The high temperature solid-state phase for $BaTiO_3$ is hexagonal.

As stated earlier in this report, when using a UV source (excimer laser) to irradiate and ablate target material, the energy absorbed causes rapid nonequilibrium heating. If the samples were also cooled in a non-equilibrium fashion, a nonequilibrium solid-state phase (hexagonal) may still be present at room temperature. This would explain the lack of a ferroelectric and nonlinear optical response, since $BaTiO_3$ is neither ferroelectric nor photorefractive in the solid-state phases cubic and hexagonal, which, in equilibrium, exist above the Curie temperature of about 130°C. The x-ray diffraction pattern for this sample may be indicative of heteroepitaxy where the hexagonal grains of $BaTiO_3$ are orienting themselves with the cubic (100) $SrTiO_3$ substrate. From the photomicrographs, it appears that the hexagonal grains are growing with the basal plane (0001) in alignment with the orientation of the single crystal $SrTiO_3$. The reactive nature of the oxygen may have also caused the formation of other barium, titanium, and oxygen compounds with different stoichiometries. This would explain those polycrystalline powder lines which

did not correlate to any form of $BaTiO_3$. Therefore, x-ray compositional analysis was performed, in an effort to gain some information on the stoichiometry of these hexagonal grains.

Data from the x-ray compositional analysis verified the existence of barium, titanium, and oxygen within the film (Fig. 51). Both ratios of interest, the intensity of the characteristic x-ray lines, the titanium Kα peak versus the barium Lα peak, and the percentage of the titanium oxide versus the barium oxide, were consistently higher than those seen with the reference standard (Fig. 52). However, with this analytical technique, quantitative results have both limited accuracy and reliability. These samples are especially difficult to analyze, because of the strong similarities between the film and the substrate.

For these perovskite structures, many dielectric and optical properties are dictated by the TiO_6^{-8} octahedron and are only slightly affected by the existing cation (barium or strontium). Last presents infrared absorption studies of several perovskite titanates ($BaTiO_3$, $SrTiO_3$, $PbTiO_3$, and $CaTiO_3$) [22]. He reveals the small discrepancies seen in the spectral data of these samples with different cations. As stated by Cardona, in a paper published on the optical properties and band structure of both $SrTiO_3$ and $BaTiO_3$ [23], the transitions between the 2p oxygen states and the 3d titanium states determine the fundamental absorption edge. Also Michel-Calendini et al. have extensively studied

the energy band structure of the ABO_3 perovskite oxides [24,25]. Their calculations verified that near the band edge, the upper levels of the valence band are occupied by the 2p oxygen states and the lower levels of the conduction band are occupied by the 3d titanium states.

If enough energy can be supplied to the film under equilibrium conditions, it should be possible to cause the nonequilibrium hexagonal phase to undergo the desired phase transitions, hexagonal to cubic then cubic to tetragonal. The sample was, therefore, placed in a furnace for a post-deposition high temperature anneal. The temperature ramp from room temperature to 1100°C (maximum furnace temp.) took place over 18 hours at a rate of 1°C/min. The slow heating process was to minimize induced stress which might lead to plastic deformation within the grains. This is undesirable, because smaller grains would form on recrystallization at the high temperatures. The sample was held at 1100°C for 6 hours and then ramped down in temperature from 1100°C to 150°C at a rate of 1°C/min. The phase transition from hexagonal to cubic is obviously of concern, however, the transition from cubic to tetragonal is critical in producing the properties of interest, especially photorefractivity. Since this phase transition takes place at the Curie temperature of approximately 130°C, where the material goes from a nonpolar phase to a polar phase ($BaTiO_3$ becomes ferroelectric), the cooling process continued at a much reduced rate of 1°C/hour over a 40 hour period, ramping down

from 150°C to 110°C. The final stage of the cooling process occurred at a rate of 1°C/min and took 1.5 hours in a ramp down from 110°C to room temperature.

After the annealing process was completed, the film was once again analyzed using the scanning electron microscope. If the desired phase transitions had taken place, the hexagonal grains should have undergone a geometric transformation to a tetragonal shape. Evidence that this actually did happen, can be seen in the photomicrographs of various grains throughout the film (Figs. 53,54). The grains, on average, do seem larger after the heat treatment. The size appears to range from about 15 microns on an edge to over 50 microns on an edge. This may have resulted from larger grains growing during the annealing process at the expense of the smaller grains. The hexagonal structure seems to collapse with edges disappearing to form a four-sided structure. Certain grains appear to have undergone only a partial transformation (Fig. 55). In one case, it is even possible to see the planar stacking (Fig. 56). The next study in this project should be to determine whether the heat treatment has had a dramatic effect on both the ferroelectric and nonlinear optical response of this sample.

OPTICAL CHARACTERIZATION:

Optical characterization refers primarily to the evaluation of the nonlinear optical response of these

samples. Of particular interest is the photorefractive sensitivity of each sample in comparison with one another and with commercially available bulk single crystals. The initial studies involve a two-beam coupling system for measuring the energy transfer between the incident waves (Fig. 57). The same experimental configuration is also utilized for the study of diffraction efficiency and optical storage in the formation and reconstruction of holograms. Phase conjugation studies will be performed after a significant photorefractive response is established within a particular sample. A pulsed Nd:YAG laser has also been coupled into the optical system in order to gather data on energy requirements and the temporal response of these films. Lam et al., in studies using the second harmonic wavelength (532 nm) of the Nd:YAG laser, have shown that nanosecond pulses can be used to generate refractive-index gratings in commercially available bulk single crystals of $BaTiO_3$ [26].

Almost all the samples have been optically characterized, even if the results from other analytical techniques were not completely favorable. The vast majority of the samples demonstrated only minimal photorefractive sensitivity. However, the most recent films made on $SrTiO_3$, which have shown encouraging results, have yet to be fully characterized. Also through discussion with certain faculty members at The Johns Hopkins Department of Materials

Science and Engineering and The Johns Hopkins Center for Nondestructive Evaluation, a much higher resolution system is being devised which should allow for optical studies to take place within each small grain (intragranularly).

POLING:

Another study involving poling techniques took place simultaneously to the film deposition work. Poling a thin film to obtain the polarization axis, c-axis, in the plane of the film can be rather challenging. A number of attempts were made attaching leads to the film surface with a pre-determined gap between them. Using a high voltage supply and heater did not produce the desired results.

A novel technique was developed using an electric field from something that approximates a point source; the field emanates from the tip of a small pin. The e-field was propagated through a single crystal commercially available 1 mm thick sample of tetragonal $BaTiO_3$ to a conductive base plate underneath. To insure the correct phase of the test material, it was evaluated optically (hologram formation and reconstruction), where its nonlinear optical response was verified.

As stated earlier, polarized light microscopy can be used to view orthogonal domains. The following photomicrographs show the material both under normal lighting conditions and when illuminated with polarized light (Figs. 58,59). The grayish features in the background

seen under polarized light are the remains of the conductive silver paint and should not be considered as part of this experiment. This material had originally been used in one of the first attempts at film deposition (homoepitaxy - no lattice mismatch). The photomicrograph showing the sample under polarized light reveals two large domains which divide the material almost in half.

The test sample was then placed on a conductive copper plate and the approximated point source was brought within 1 mm of the surface of the sample. The e-field generated at the point source propagates through the test sample to the conductive plate underneath. The effect that the e-field had on the test sample is presented in figure 60. Charges in the material responded to the presence of the e-field by re-orienting themselves and creating new domains. These domains have aligned themselves either parallel (or antiparallel) or perpendicular to one another, such that domain walls exist either at 90° or 180° to one another. It should be noted that this test took place in air and at room temperature.

It is, in fact, somewhat easier to take a large domain and convert to many smaller domains, then it is to go in the other direction. However, it still seems apparent that the e-field generated with this novel technique is sufficient to influence charge migration within the material. Switching of the domains does occur at temperatures below the Curie point, when the e-field applied to the sample is greater

than the coercive field. More research needs to be conducted in order to determine if the effect generated at the sample can be better controlled. More intimate contact (rather than an air gap) to improve conductivity between the base plate and the sample would minimize depolarization fields. Also putting a bias charge on the base plate should allow for greater selectivity in the characteristics of the incident e-field.

VI. CONCLUSIONS:

The progress that has taken place during this past year has brought the research project much closer to accomplishing those objectives stated at the beginning of this report, namely the processing, evaluation, and characterization of high optical quality photorefractive films of $BaTiO_3$. The results presented within this report do indicate that the research is at a very positive but critical point. The pulsed laser deposition technique has been developed to the extent that heteroepitaxial films are now being deposited and their existence verified by a variety of analytical methods. This is a tremendous advancement from the amorphous and polycrystalline films originally deposited. Also the metallo-organic decomposition technique has just recently gotten underway, and plans are to simultaneously study RF and DC sputtering as another thin film processing alternative. Access has

already been granted for use of a new 3-gun and 5-head sputtering system at the Army Research Lab at Fort Belvoir.

These preliminary results have produced interest in this research from other Federal Agencies and Universities. As stated earlier, the Army Research Lab has been of assistance in a variety of ways. Also the National Security Agency has recently awarded a small contract for similar research on the sillenite materials, bismuth silicon oxide - $Bi_{12}SiO_{20}$, bismuth titanium oxide - $Bi_{12}TiO_{20}$, and bismuth germanium oxide - $Bi_{12}GeO_{20}$, in a collaborative effort between The Johns Hopkins Applied Physics Laboratory, the Department of Materials Science and Engineering (Homewood Campus), and the Center for Nondestructive Evaluation (Homewood Campus). Access to other analytical equipment and the expertise in various optical techniques for materials characterization at The Johns Hopkins Homewood Campus should strengthen this program immensely. However, even with the favorable research results and the establishment of the collaborative efforts, the funding for this program is greatly diminishing. If additional funding sources do not become available, budgetary constraints may force the project come to an end at this critical juncture.

The principal investigator would like to acknowledge the assistance given by Dr. Tom Kistenmacher of The Johns Hopkins Applied Physics Laboratory in the area of x-ray diffraction and also the support and technical assistance of Dr. Sharon Welch of The NASA Langley Research Center.

VII. REFERENCES:

1) J. Cheung and J. Horwitz, Mater. Res. Soc. Bull., February, 30 (1992).

2) C.L. Chan and J. Mazumder, J. Appl. Phys. **62** (11), 4579 (1987).

3) G.M. Davis and M.C. Gower, Appl. Phys. Lett. **55** (2), 112 (1989).

4) C.B. Sawyer and C.H. Tower, Phys. Rev. **35**, 269 (1930).

5) A.S. Shaikh and G.M. Vest, J. Am. Ceram. Soc. **69** (9), 682 (1986).

6) K.E. Youden, R.W. Eason, M.C. Gower, and N.A. Vainos, Appl. Phys. Lett. **59** (16), 1929 (1991).

7) D.B. Geohegan, Appl. Phys. Lett. **60** (22), 2732 (1992).

8) D. Roy, C.J. Peng, and S.B. Krupanidhi, Appl. Phys. Lett. **60** (20), 2478 (1992).

9) D. Roy and S.B. Krupanidhi, Appl. Phys. Lett. **61** (17), 2057 (1992).

10) Technical Information - Material Safety Data Sheet supplied by Solon Technologies, Inc.

11) G.K. Hubler, Mater. Res. Soc. Bull., February, 26 (1992).

12) C.S. Chern, J. Zhao, L. Luo, P. Lu, Y.Q. Li, P. Norris, B. Kear, F. Cosandey, C.J. Maggiore, B. Gallois, and B.J. Wilkens, Appl. Phys. Lett. **60** (9), 1144 (1992).

13) L.A. Wills, B.W. Wessels, D.S. Richeson, and T.J. Marks, Appl. Phys. Lett. **60** (1), 41 (1992).

14) R.W. Simon, C.E. Platt, A.E. Lee, G.S. Lee, K.P. Daly,

M.S. Wire, J.A. Luine, and M. Urbanik, Appl. Phys. Lett. **53** (26), 2677 (1988).

15) Data and Technical Information supplied by Commercial Crystal Laboratories, Inc.

16) Data and Technical Information supplied by Union Carbide Coatings Service Corporation.

17) S.H. Wemple, Phys. Rev. B **2** (7), 2679 (1970).

18) C.H. Perry, B.N. Khanna, and G. Rupprecht, Phys. Rev. **135** (2A), A408 (1964).

19) S.H. Liou and C.Y. Wu, Appl. Phys. Lett. **60** (22), 2803 (1992).

20) B.D. Cullity, Elements of X-Ray Diffraction (Addison-Wesley Publishing Co., Reading, 1959) pp. 260-261.

21) Powder Diffraction File - Inorganic Sets 1-5, edited by L.G. Berry (Joint Committee on Powder Diffraction Standards, Philadelphia, 1974) p. 654.

22) J.T. Last, Phys. Rev. **105** (6), 1740 (1957).

23) M. Cardona, Phys. Rev. **140** (2A), A651 (1965).

24) F.M. Michel-Calendini, H. Chermette, and J. Weber, J. Phys. C: Solid St. Phys. **13**, 1427 (1980).

25) F.M. Michel-Calendini, L. Hafid, G. Godefroy, and H. Chermette, Solid State Commun. **54**, 951 (1985).

26) L.K. Lam, T.Y. Chang, J. Feinberg, and R.W. Hellwarth, Opt. Lett. **6** (10), 475 (1981).

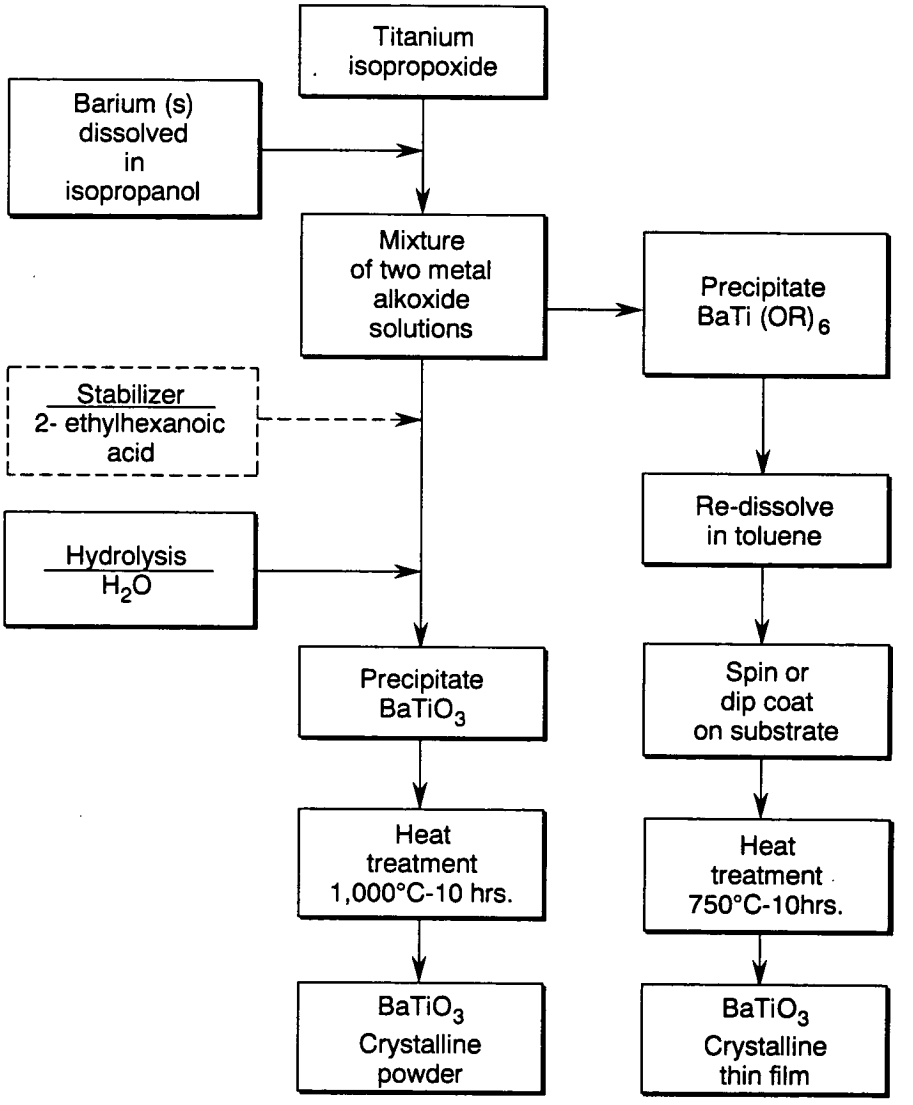

Figure 1. Flow chart describing the sol-gel method for processing $BaTiO_3$ in both the powder and thin film forms.

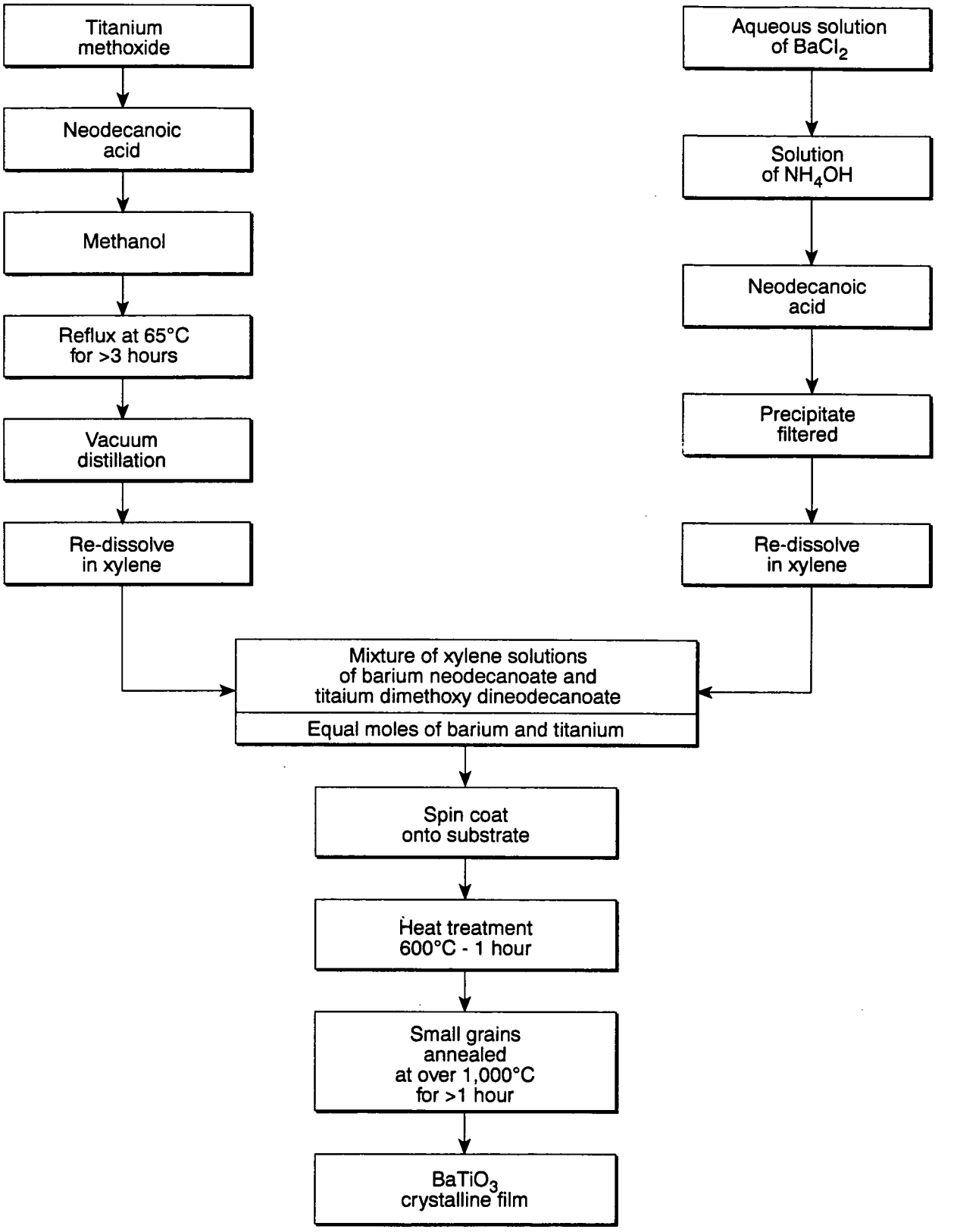

Figure 2. Flow chart describing the metallo-organic decomposition technique for processing films of $BaTiO_3$.

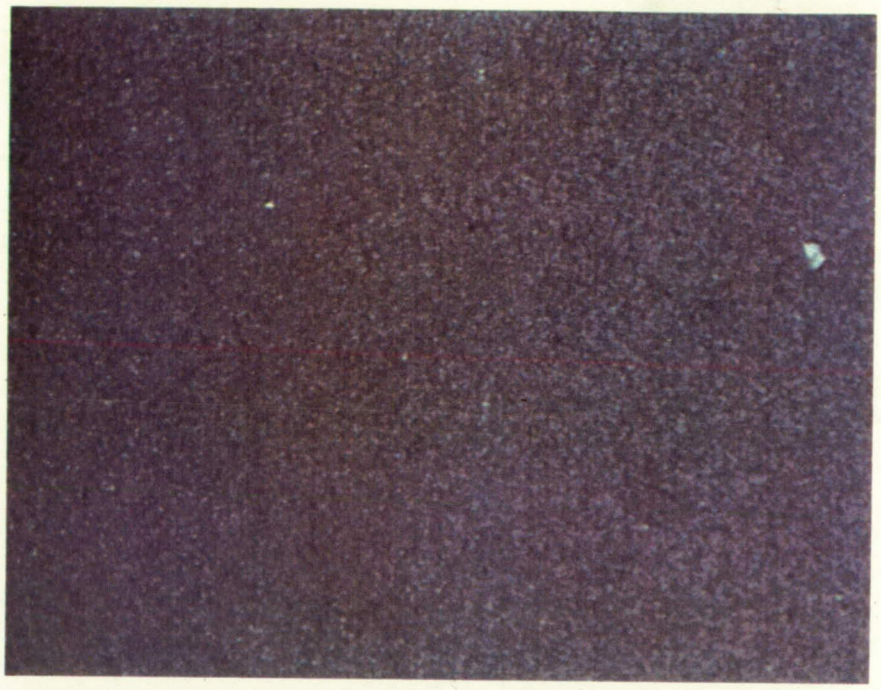

Figure 3. Photomicrograph of $BaTiO_3$ film on SiO_2 at 50x magnification before heat treatment.

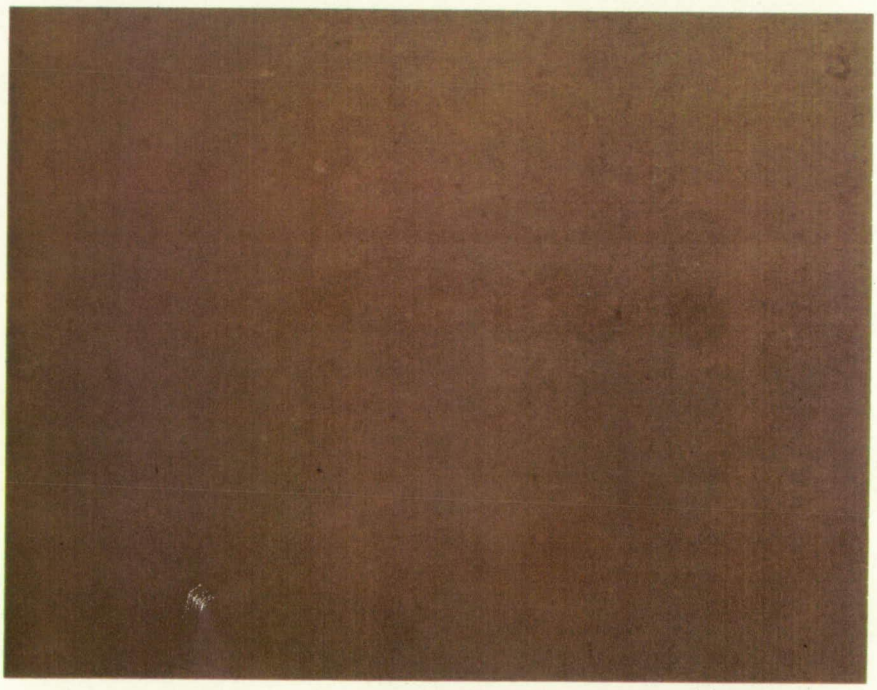

Figure 4. Photomicrograph of $BaTiO_3$ film on SiO_2 at 50x magnification after heat treatment.

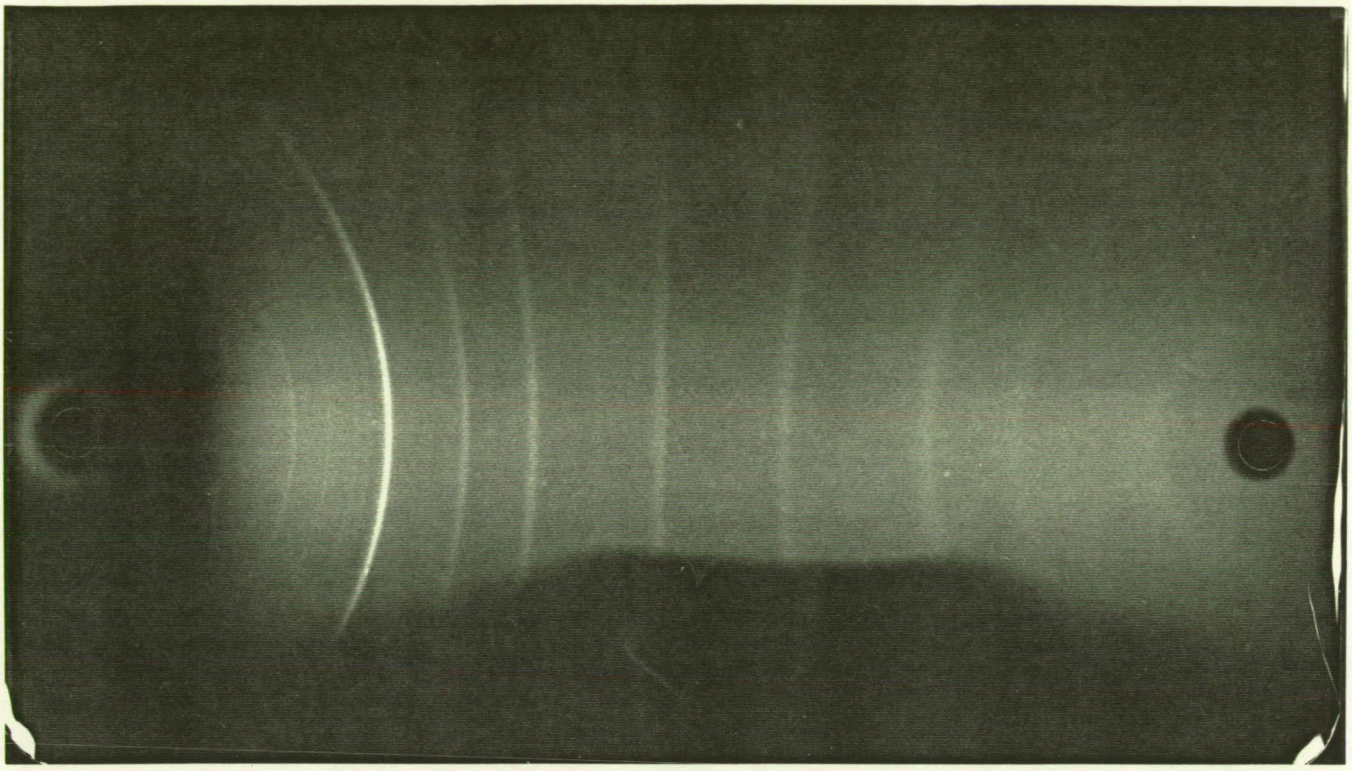

Figure 5. X-ray diffraction pattern from a $BaTiO_3$ film on SiO_2 indicates polycrystallinity.

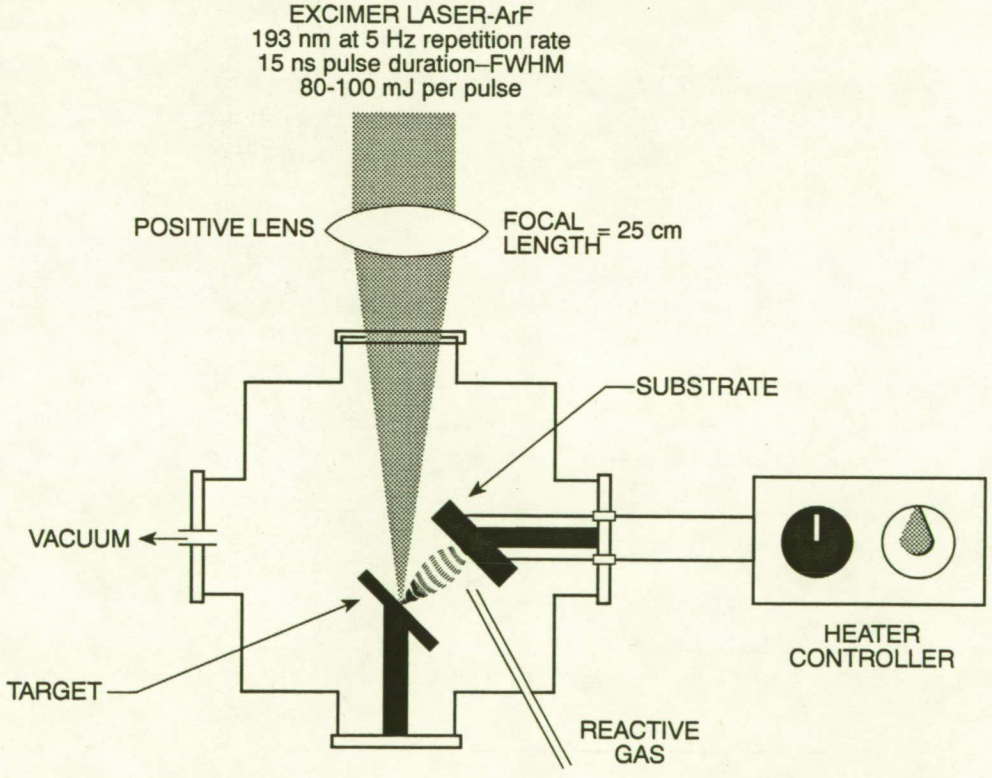

Figure 6. Schematic drawing of the pulsed laser deposition process.

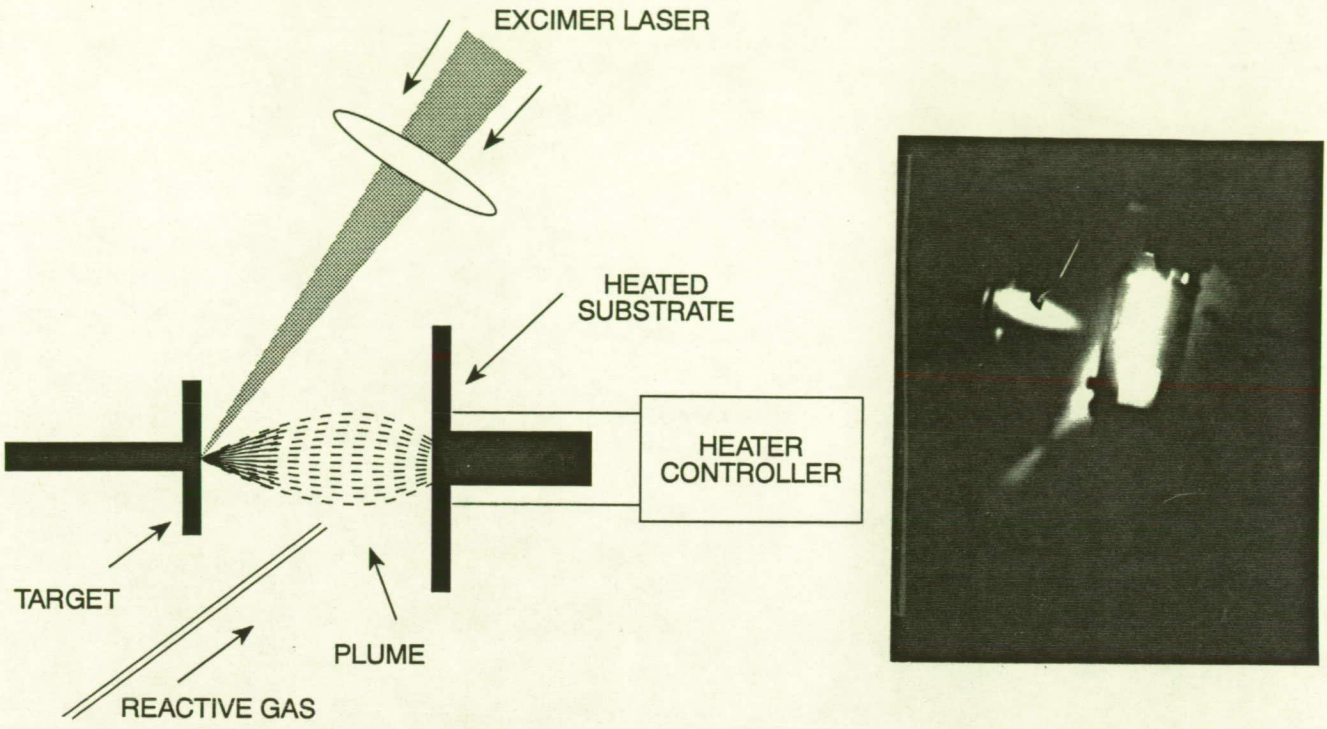

Figure 7. Schematic drawing and photograph taken inside the vacuum chamber of the pulsed laser deposition technique taking place. The plume is formed and directed onto a heated substrate.

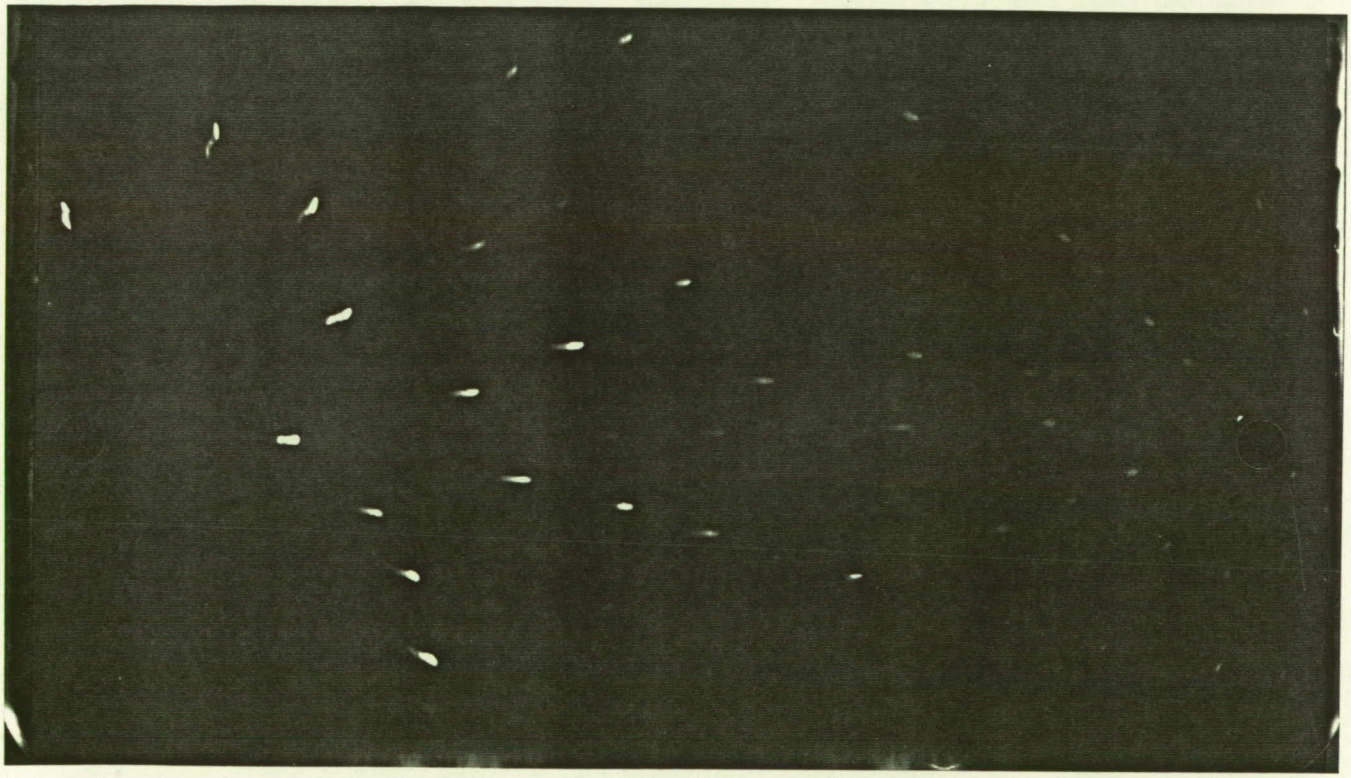

Figure 8. X-ray diffraction pattern of a (100) single crystal LiF substrate with cubic crystallinity.

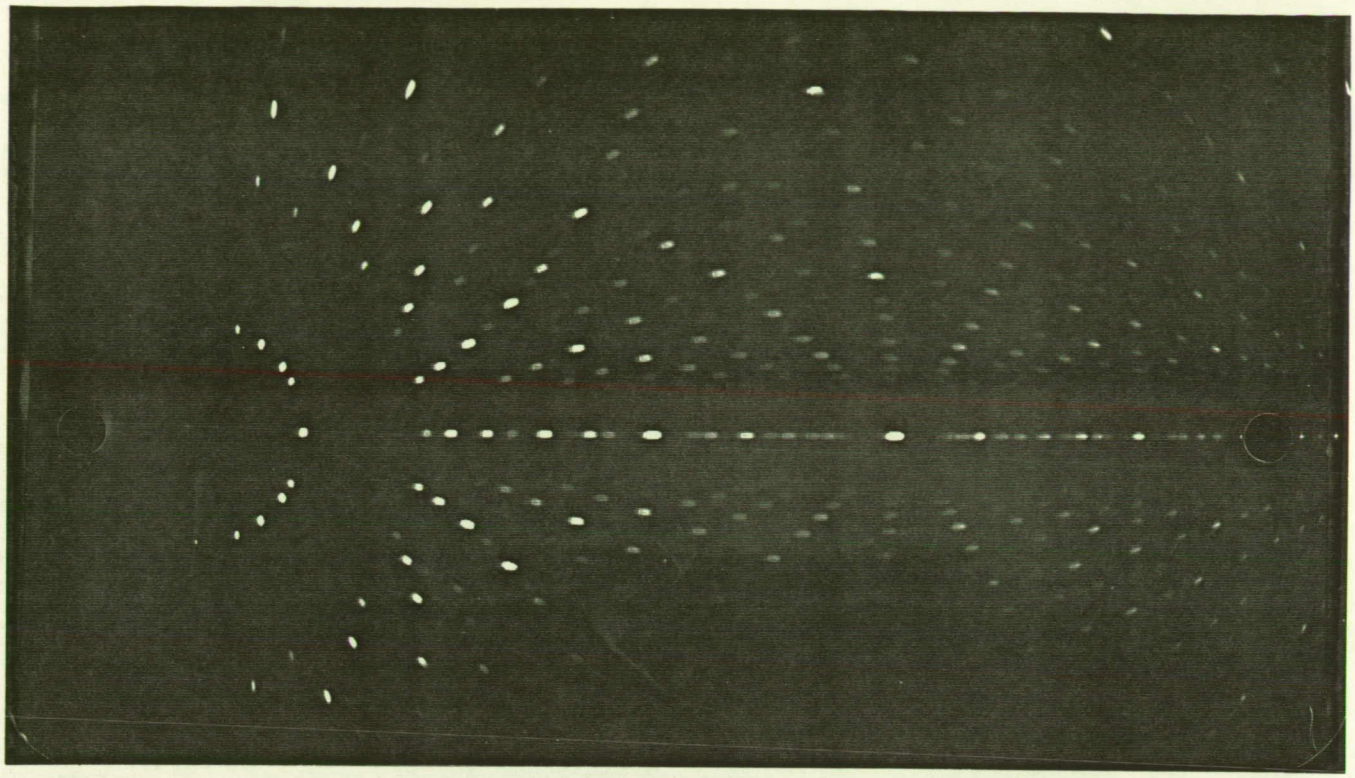

Figure 9. X-ray diffraction pattern of a (100) single crystal $LaAlO_3$ substrate with a slight rhombohedral distortion from cubic crystallinity.

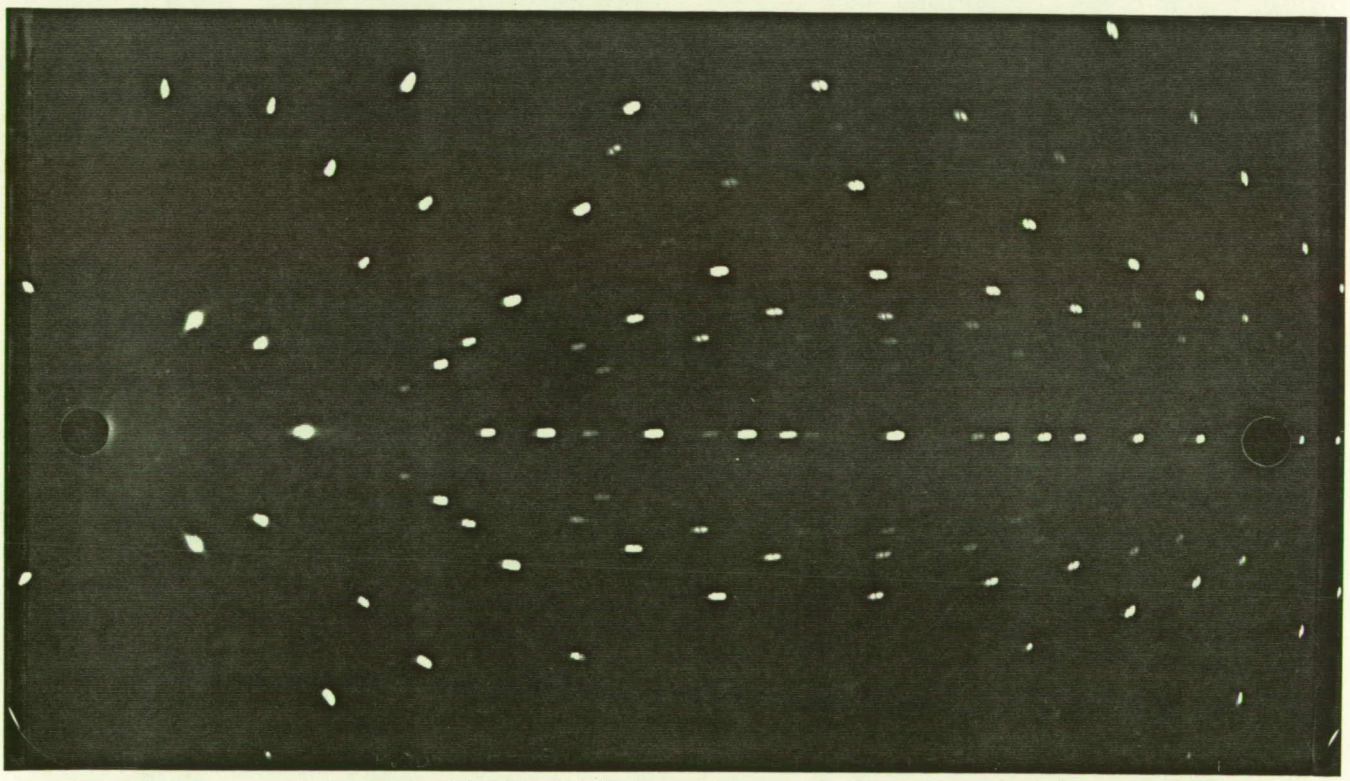

Figure 10. X-ray diffraction pattern of a (100) single crystal MgO substrate with cubic crystallinity.

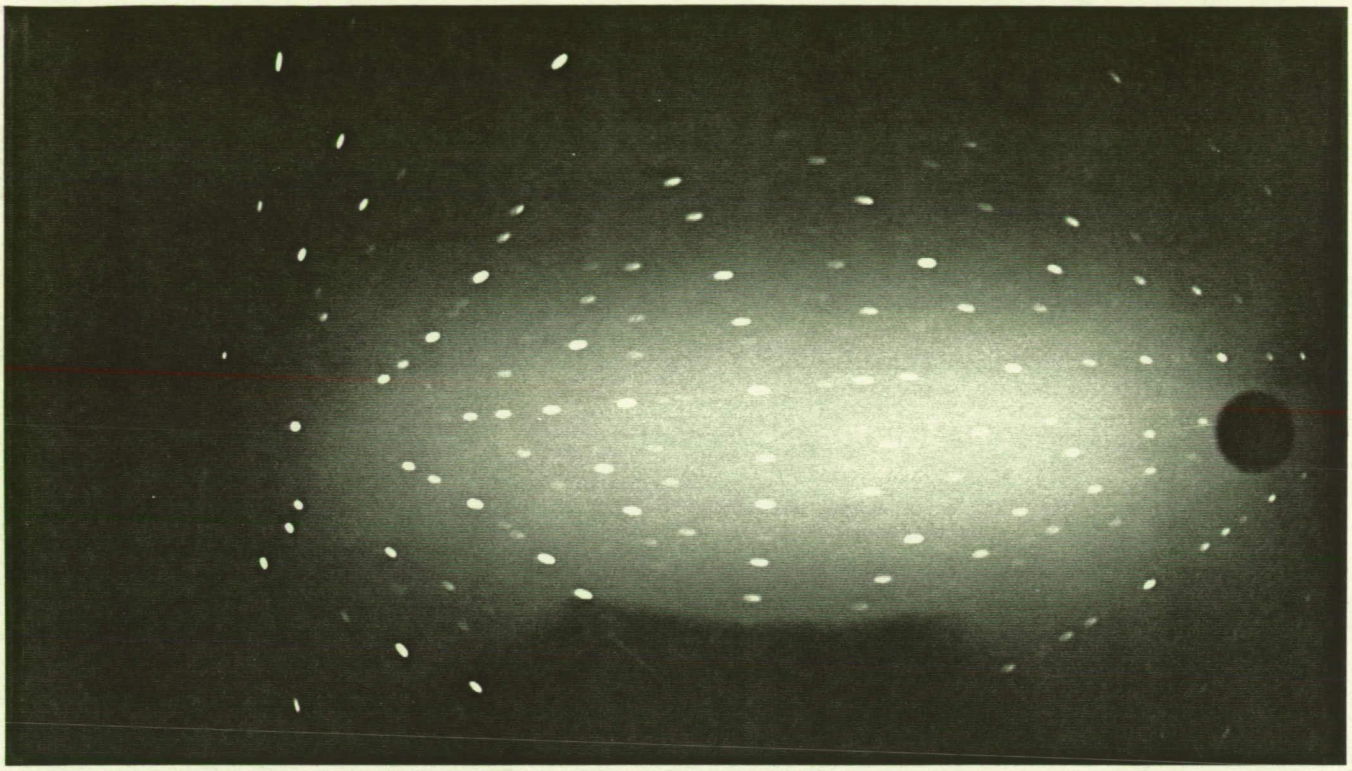

Figure 11. X-ray diffraction pattern of a cubic (100) single crystal $SrTiO_3$ substrate.

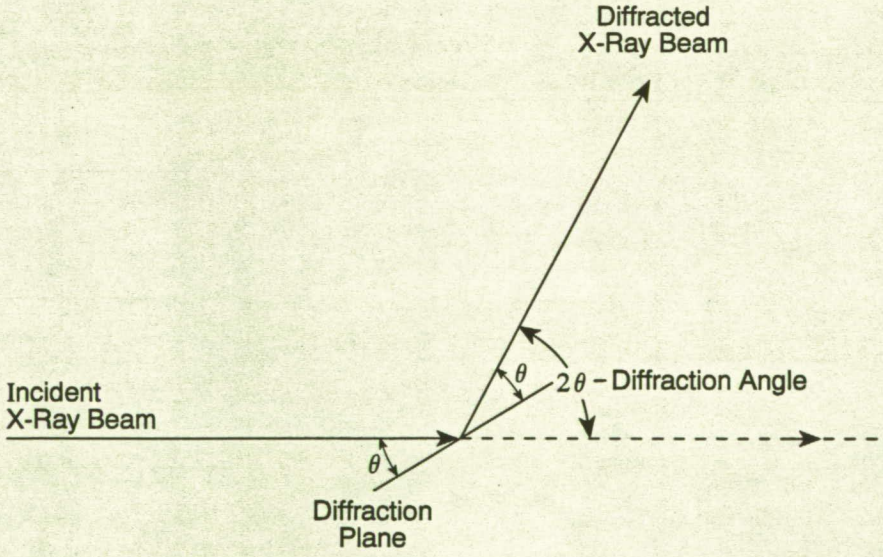

Figure 12. Schematic drawing of the angular relationship between the incident x-ray beam and those planes which satisfy Bragg's Law (diffraction planes).

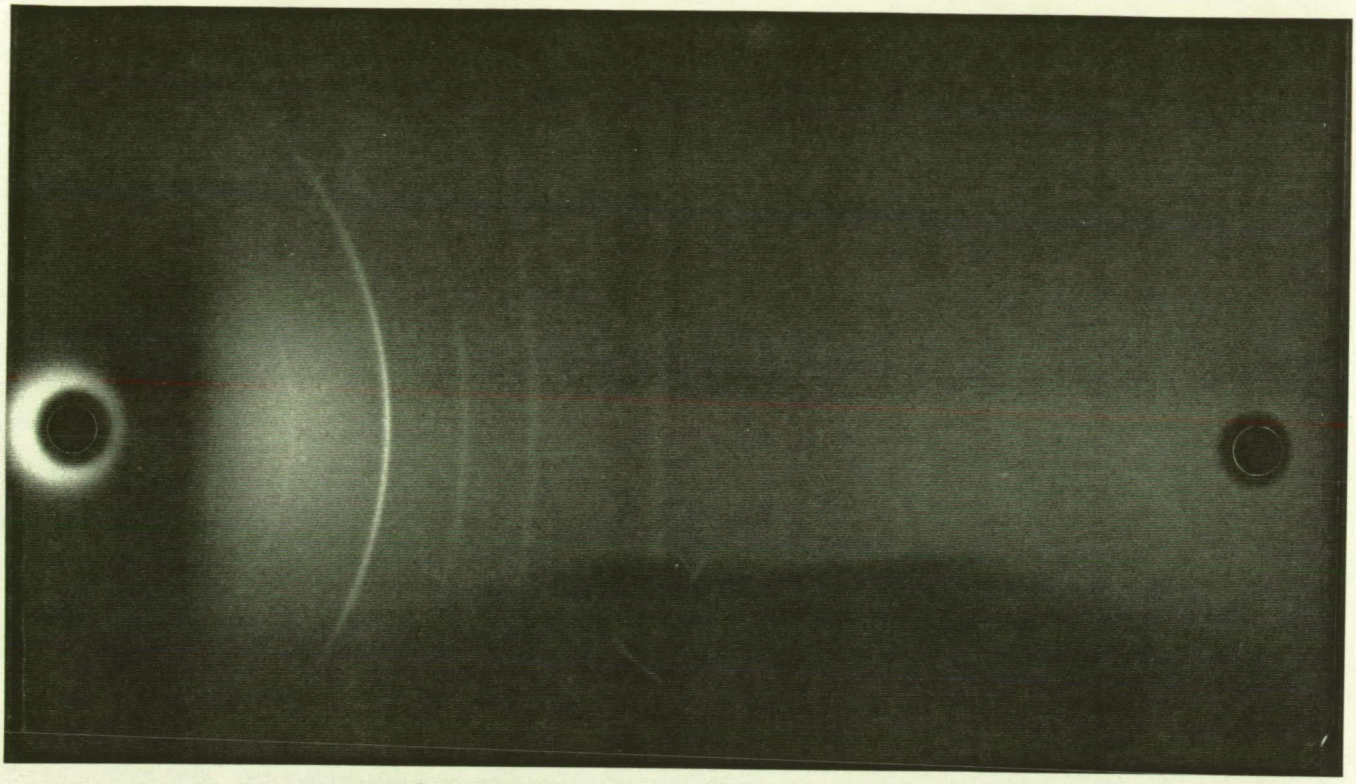

Figure 13. Sample x-ray diffraction pattern indicating a polycrystalline film.

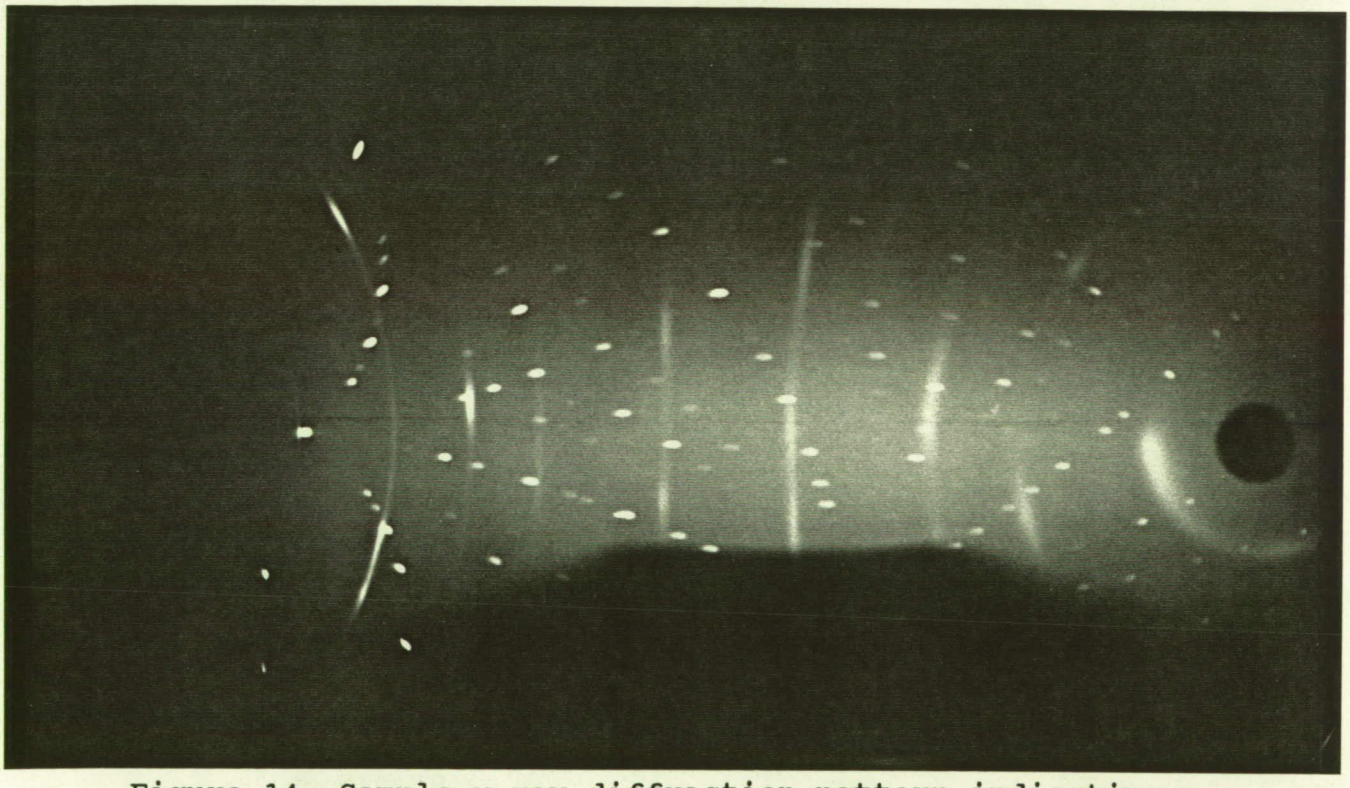

Figure 14. Sample x-ray diffraction pattern indicating a polycrystalline film with texture.

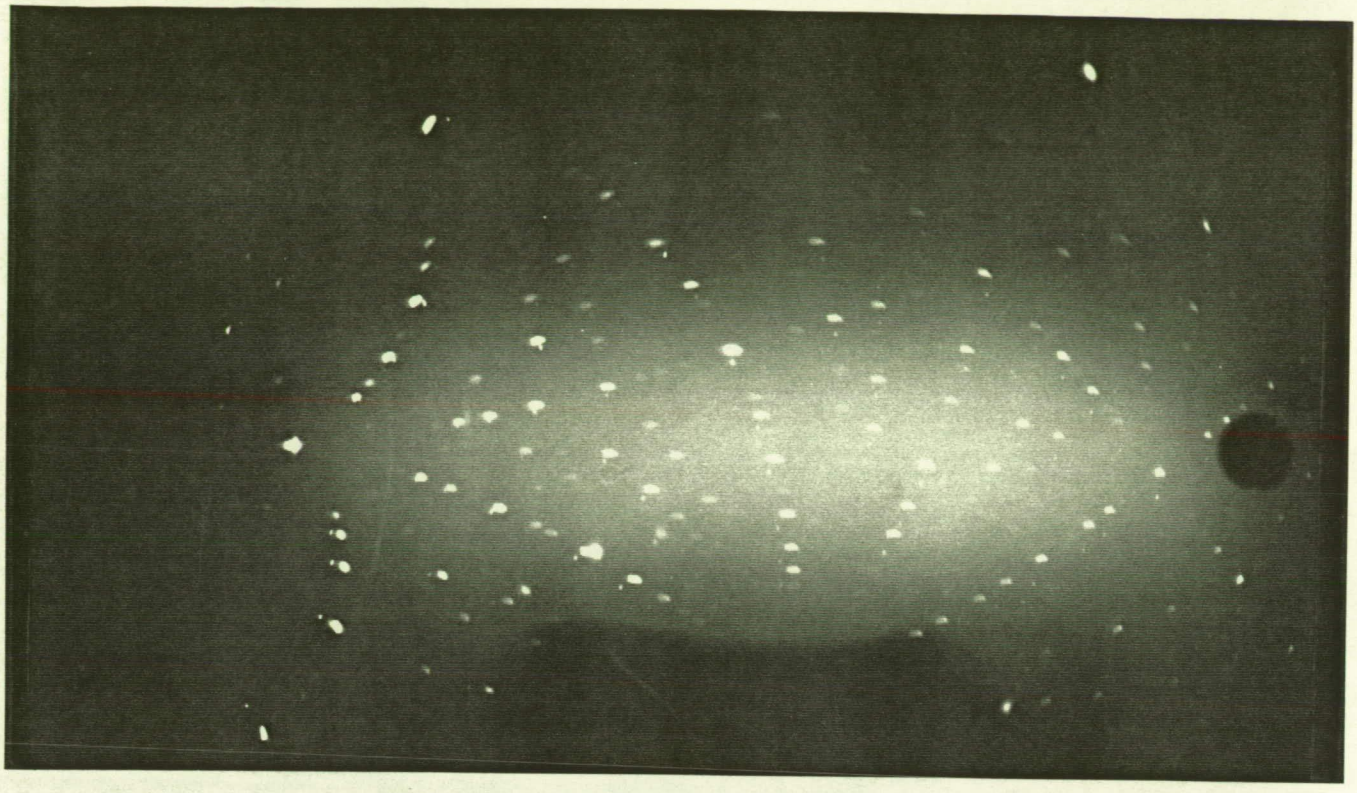

Figure 15. Sample x-ray diffraction pattern indicating heteroepitaxial film growth.

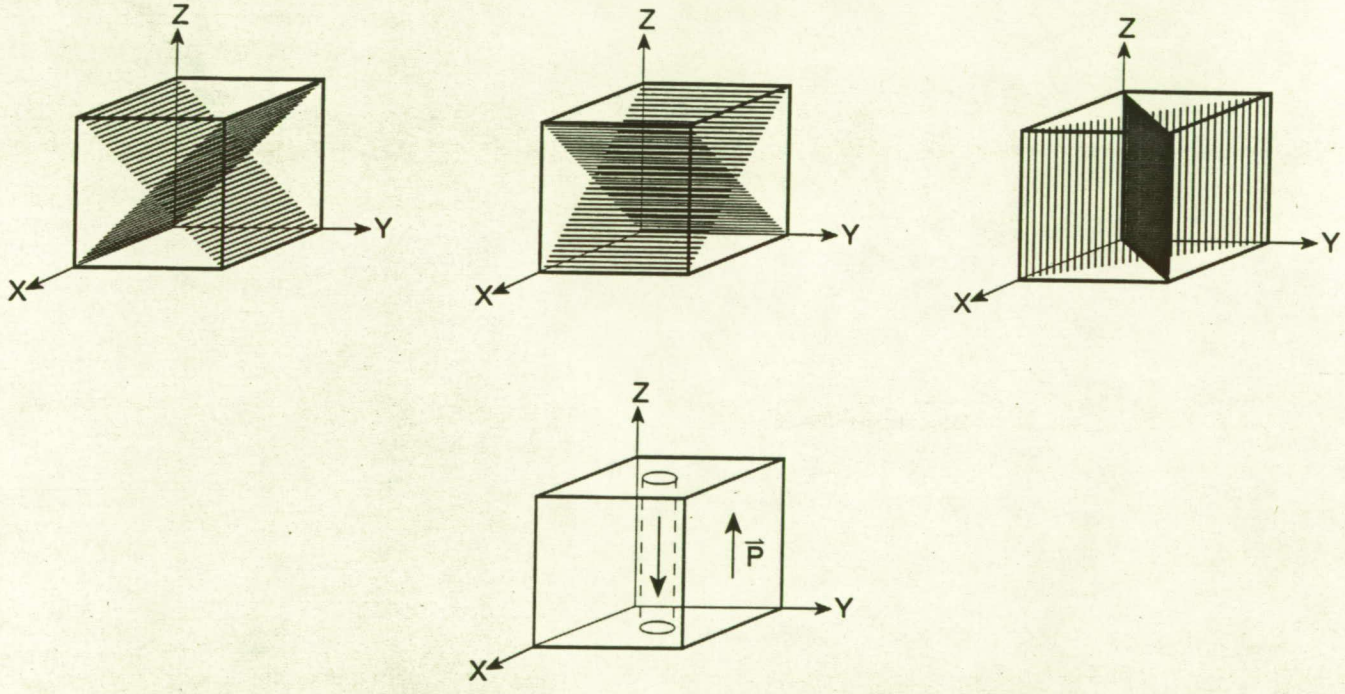

Figure 16. Schematic drawing of the domains formed within $BaTiO_3$ during the phase transition at the Curie temperature.

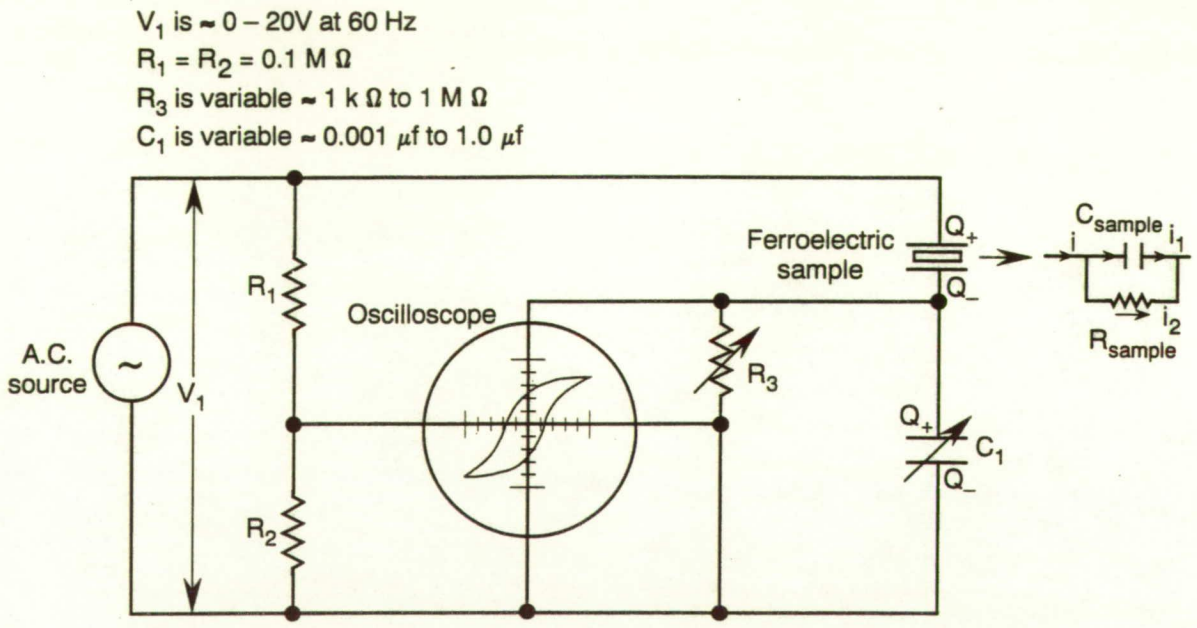

Figure 17. Schematic drawing of a modified Sawyer-Tower circuit for performing ferroelectric analysis.

Figure 18. Photomicrograph of the remaining section of the $BaTiO_3$ film on an LiF substrate after the deposition process.

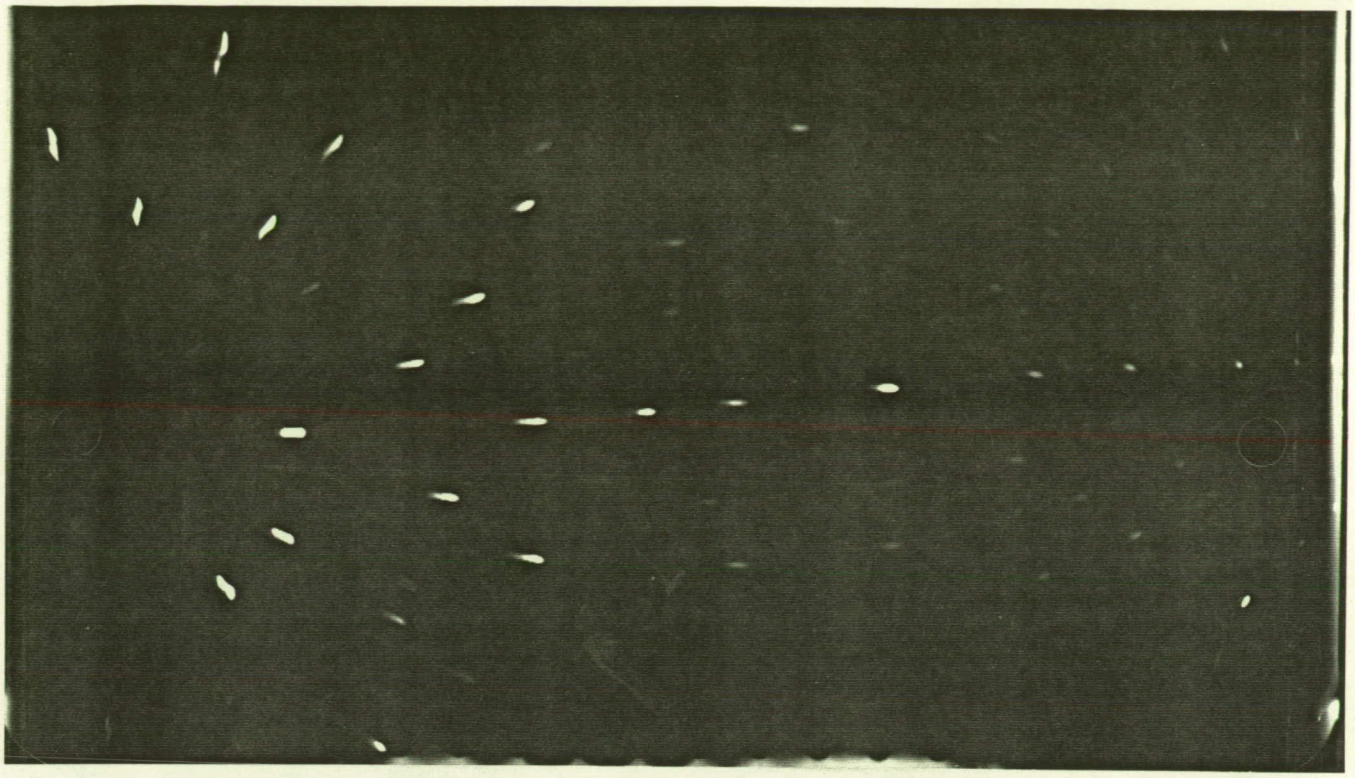

Figure 19. X-ray diffraction pattern indicating only the LiF substrate material (no $BaTiO_3$ film).

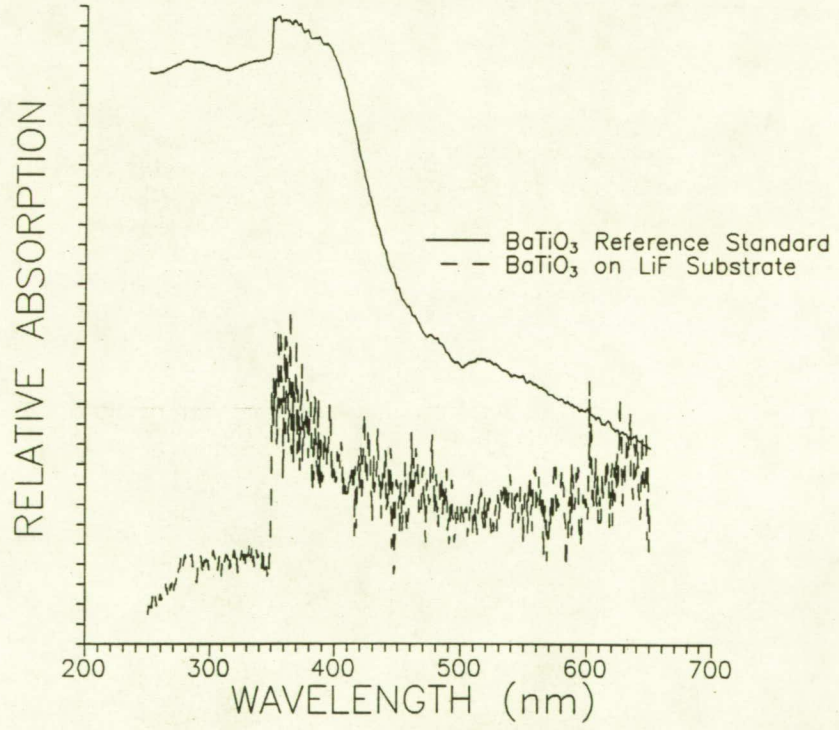

Figure 20. Spectral data from the UV-Vis spectrometer indicate only the existence of the LiF substrate (no $BaTiO_3$ film).

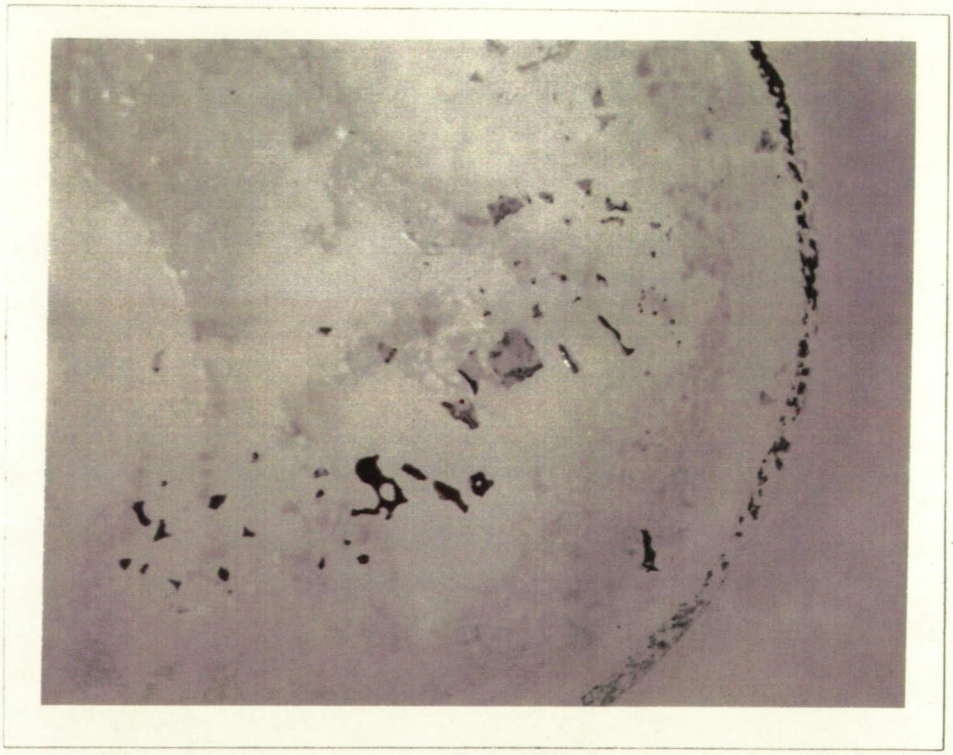

Figure 21. Photomicrograph of the remaining sections of the $BaTiO_3$ film on LiF after the deposition process.

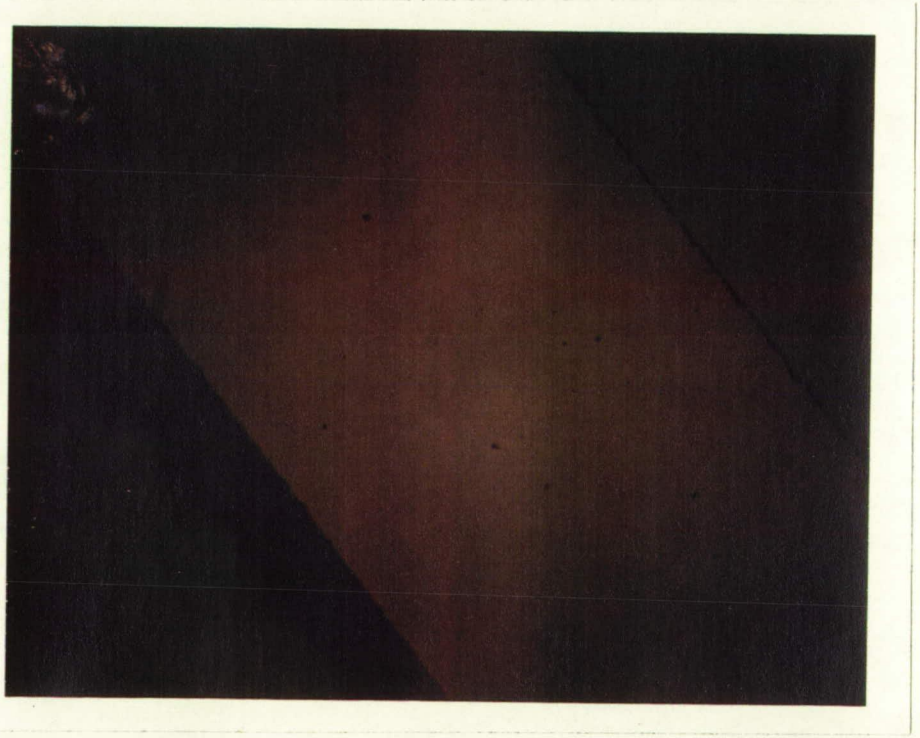

Figure 22. Photomicrograph of a $BaTiO_3$ film on a $LaAlO_3$ substrate.

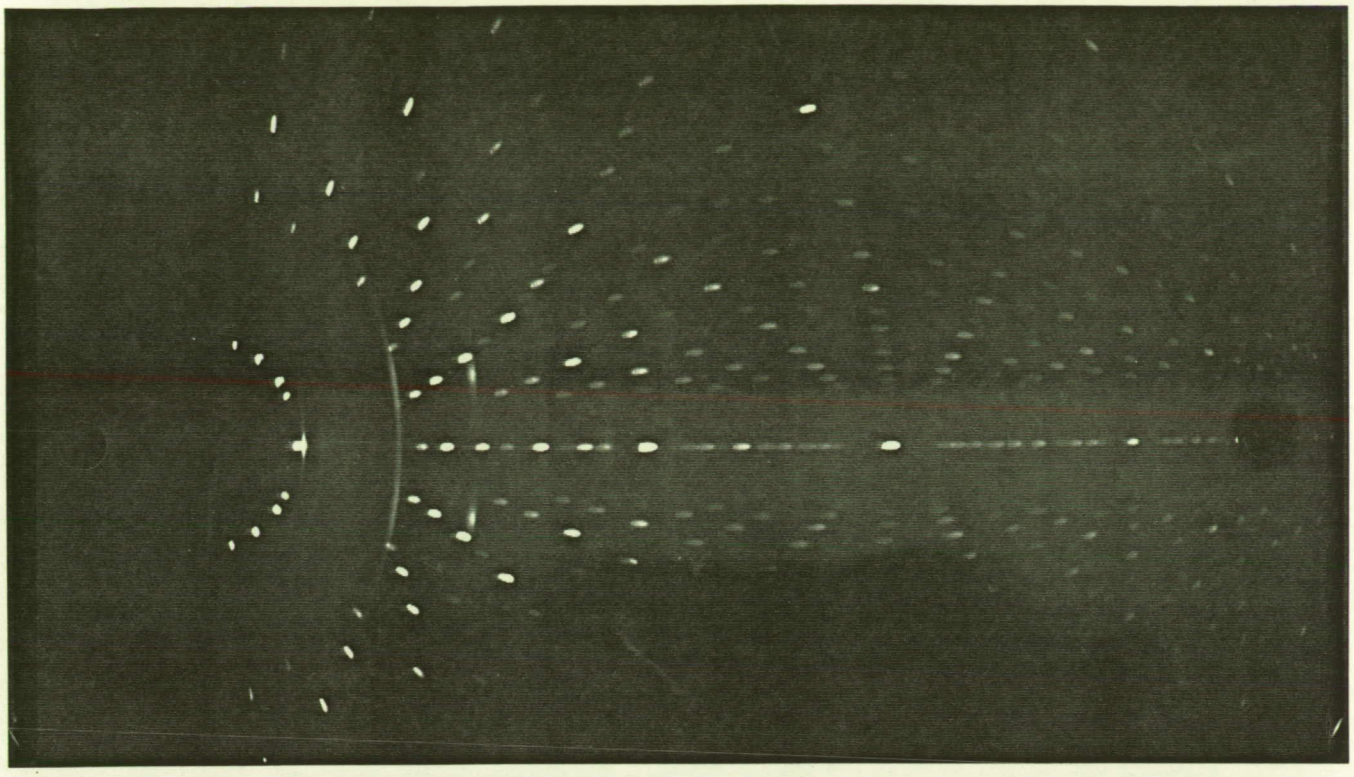

Figure 23. X-ray diffraction pattern from a $BaTiO_3$ film on $LaAlO_3$ indicates a polycrystalline sample with some preferred orientation.

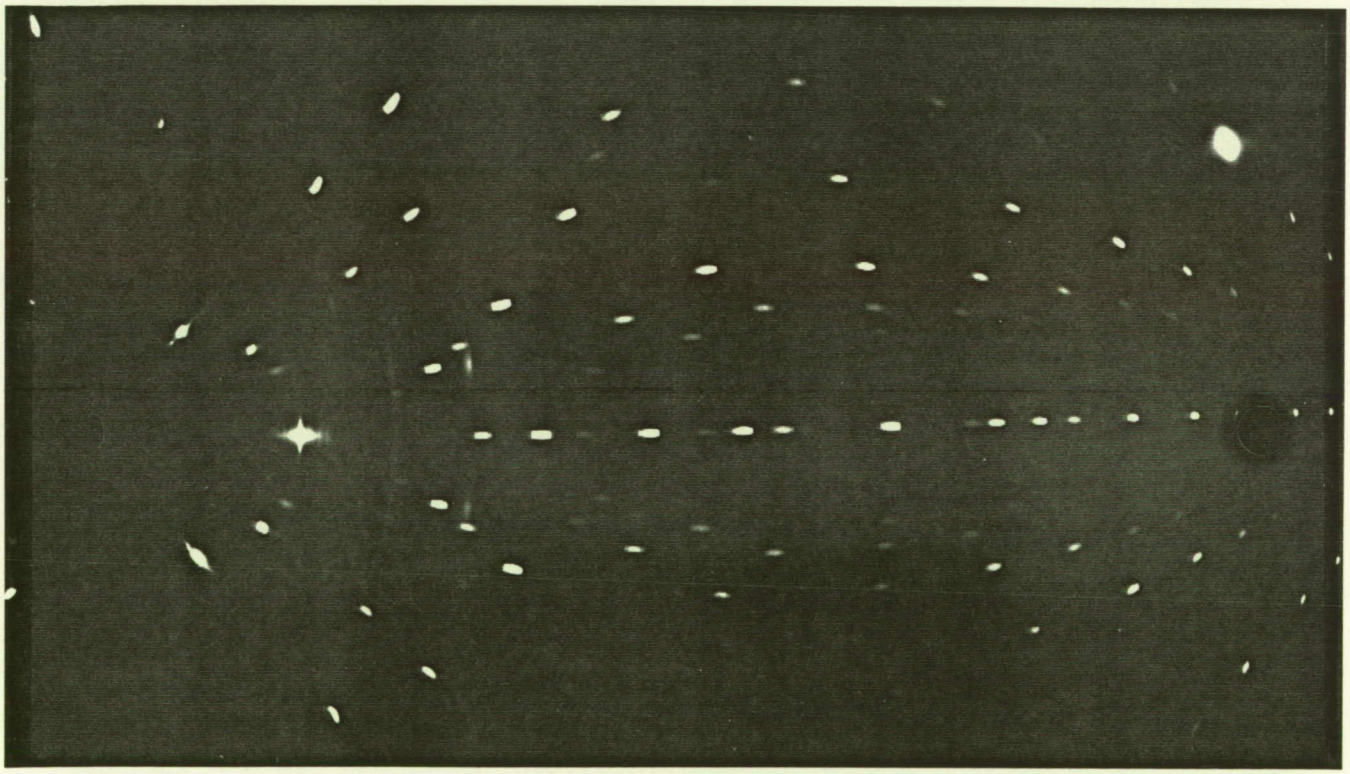

Figure 24. X-ray diffraction pattern from a $BaTiO_3$ film on MgO indicates a polycrystalline sample with preferential orientation.

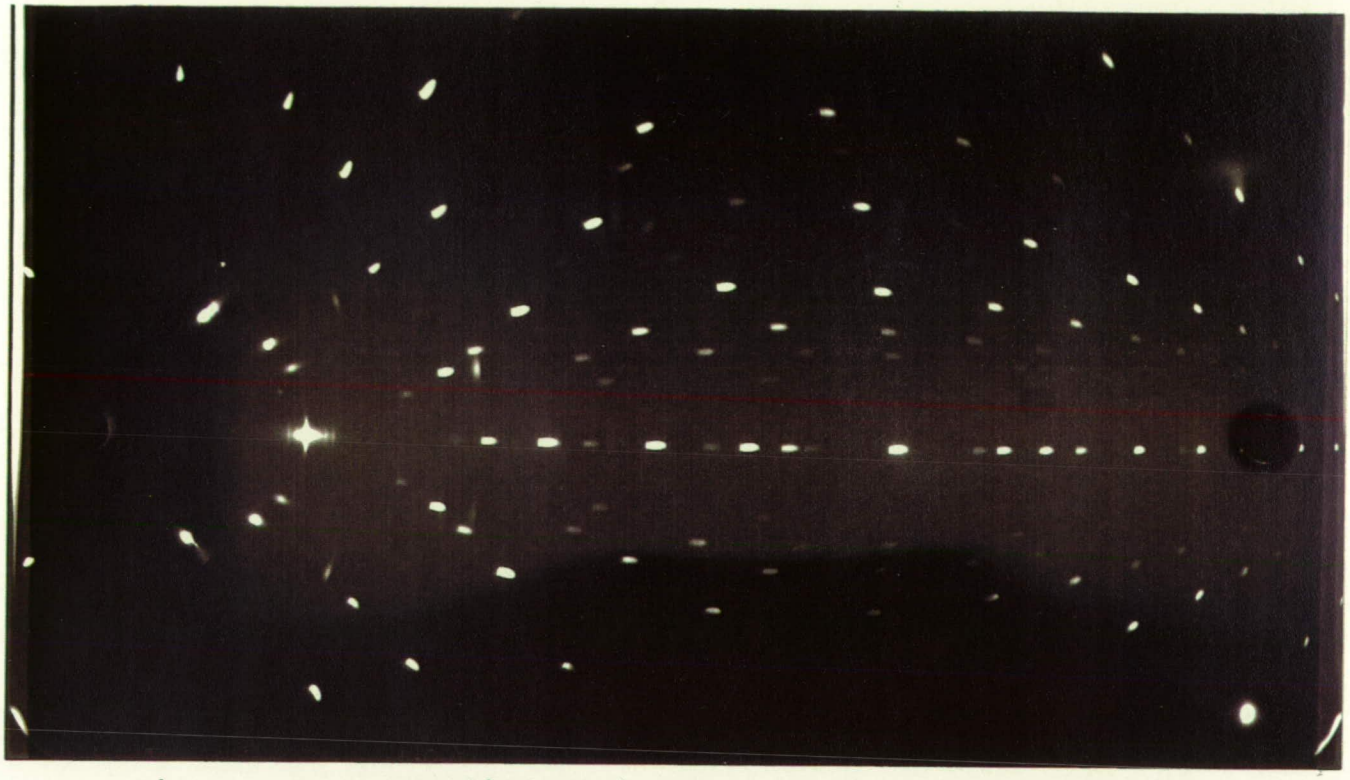

Figure 25. X-ray diffraction pattern taken after heat treatment of a $BaTiO_3$ film on MgO demonstrates minimal change as a result of the annealing process.

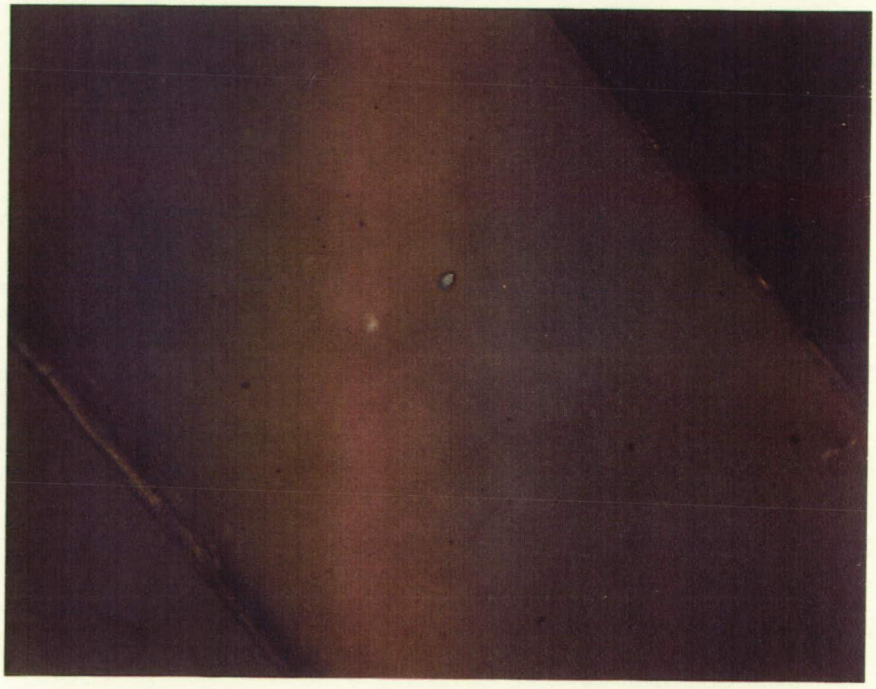

Figure 26. Photomicrograph of a typical 1 micron thick $BaTiO_3$ film on MgO.

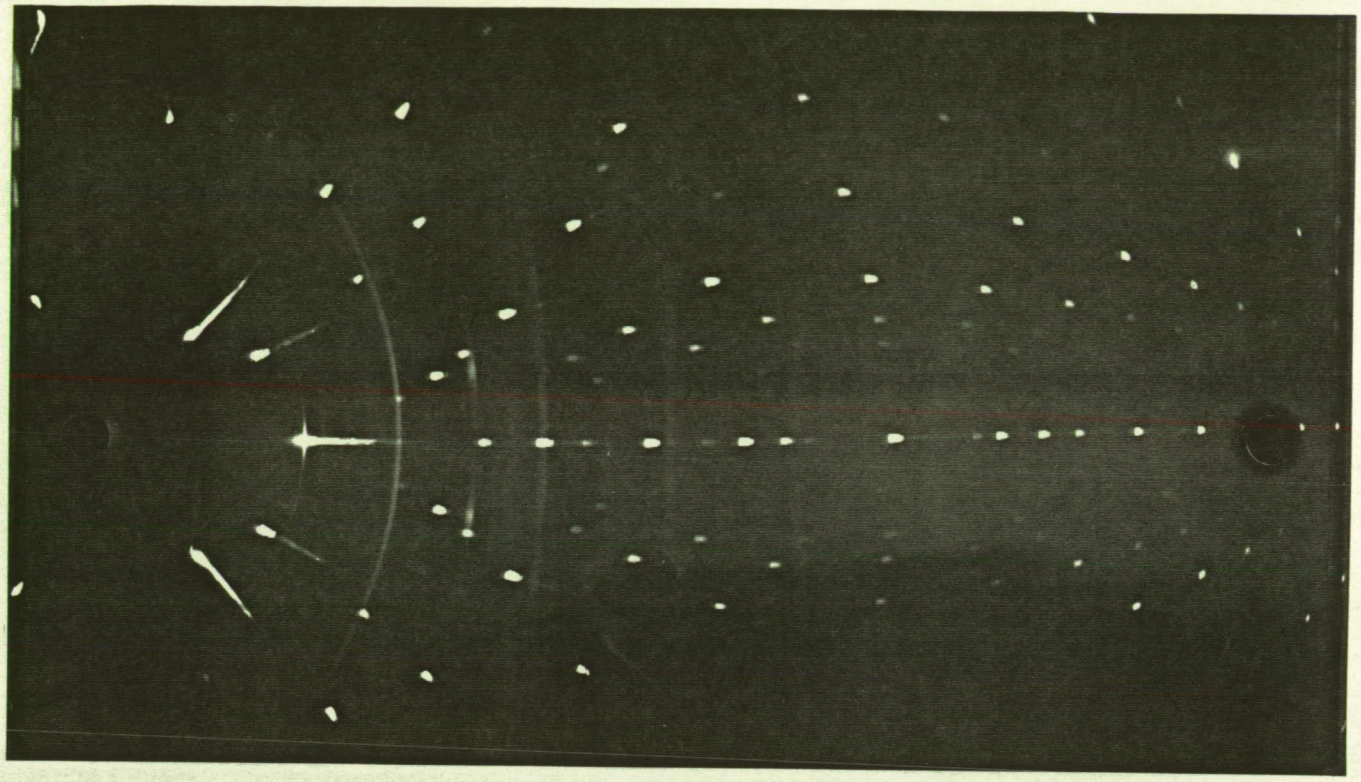

Figure 27. Typical x-ray diffraction pattern resulting from variations in the deposition parameters for $BaTiO_3$ on MgO. The x-ray data indicates no improvement in crystallinity.

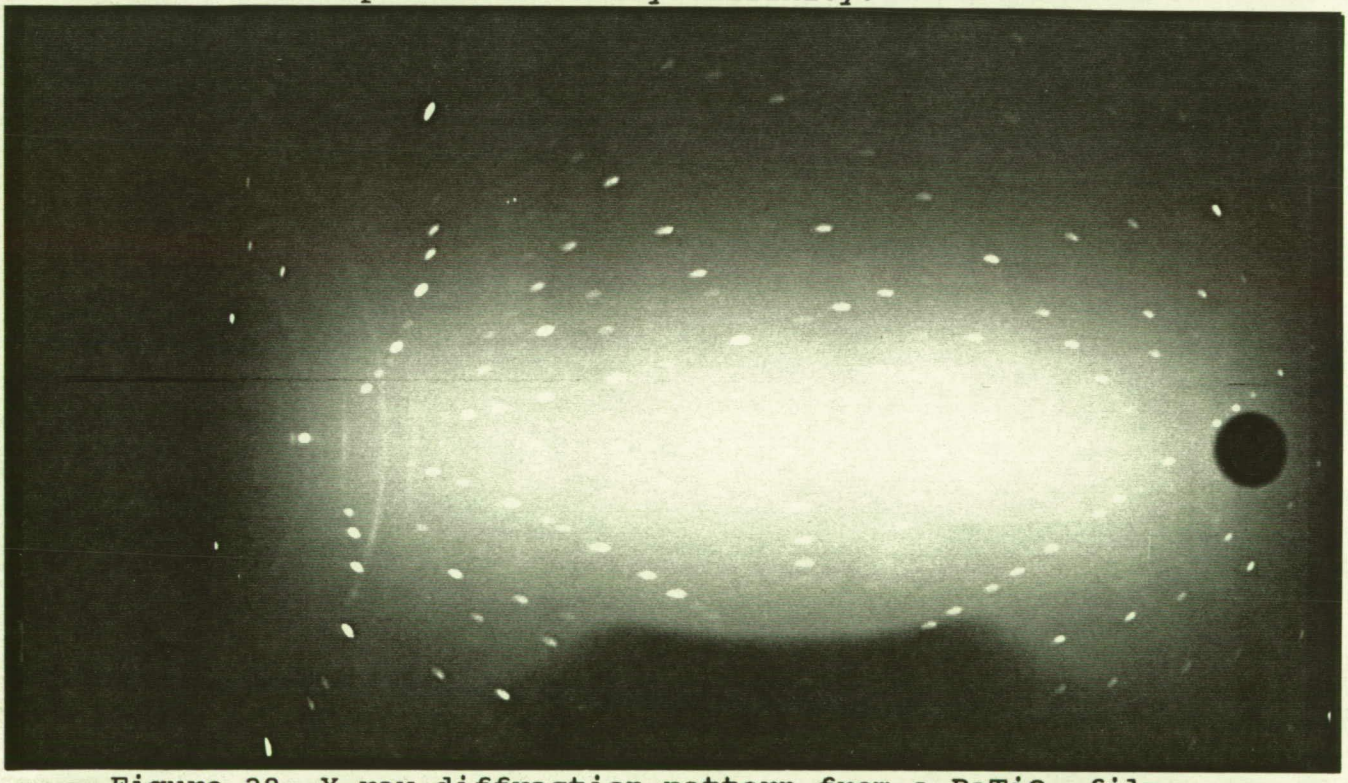

Figure 28. X-ray diffraction pattern from a $BaTiO_3$ film deposited on $SrTiO_3$ at 600°C exhibits only slight indications of crystallinity.

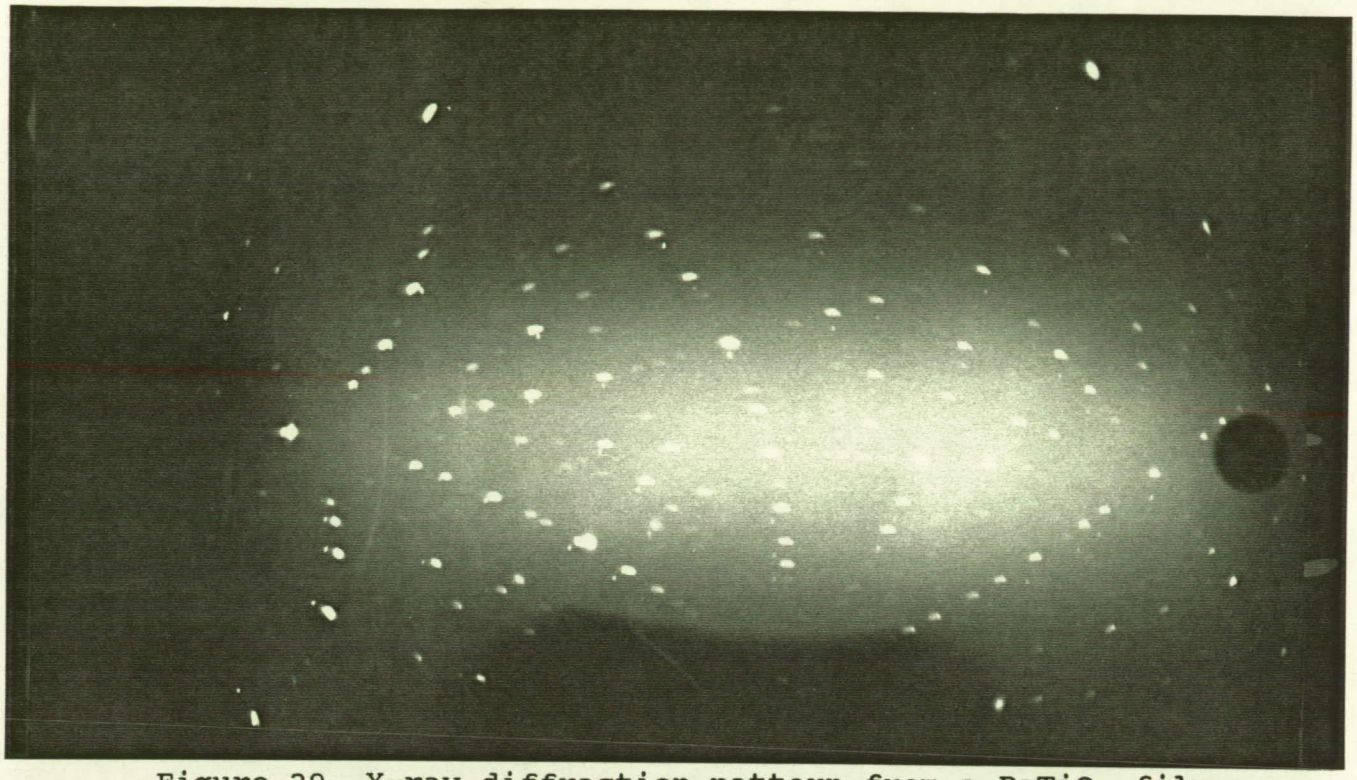

Figure 29. X-ray diffraction pattern from a $BaTiO_3$ film deposited on $SrTiO_3$ at 800°C exhibits some indications of heteroepitaxial growth.

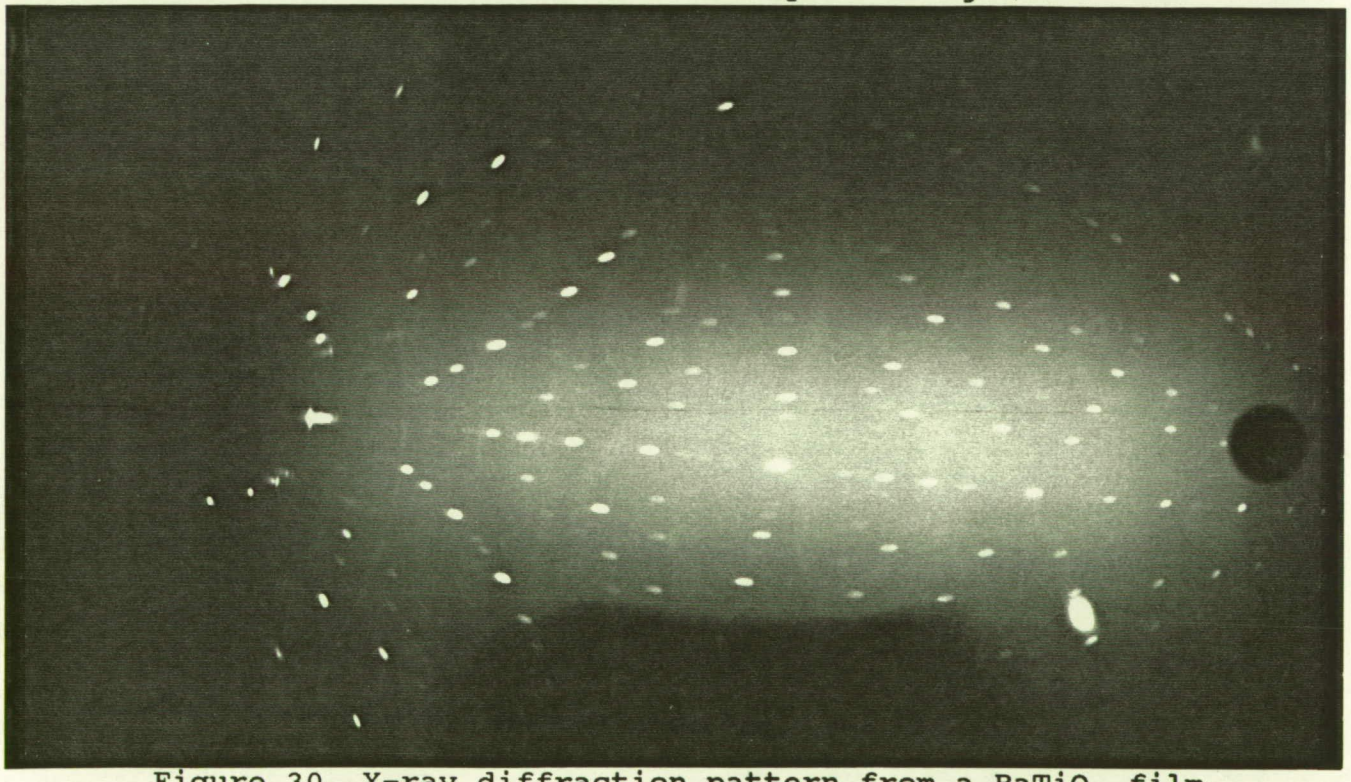

Figure 30. X-ray diffraction pattern from a $BaTiO_3$ film deposited on $SrTiO_3$ at 900°C shows no major improvement in crystallinity over the film deposited at 800°C.

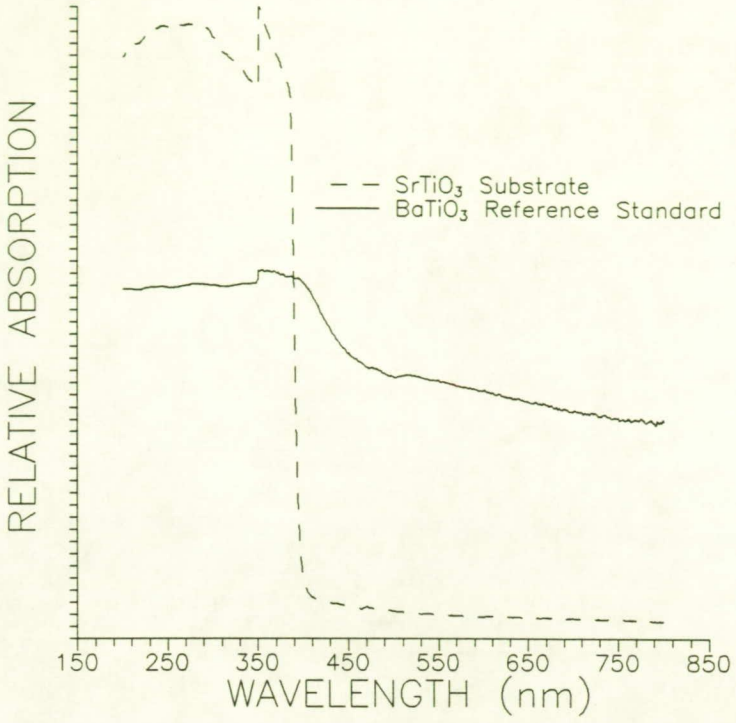

Figure 31. UV-Vis spectrometer data shows the absorption characteristics for single crystal samples of $BaTiO_3$ and $SrTiO_3$ over the spectral range of 200 nm to 800 nm (absorption tail on $BaTiO_3$).

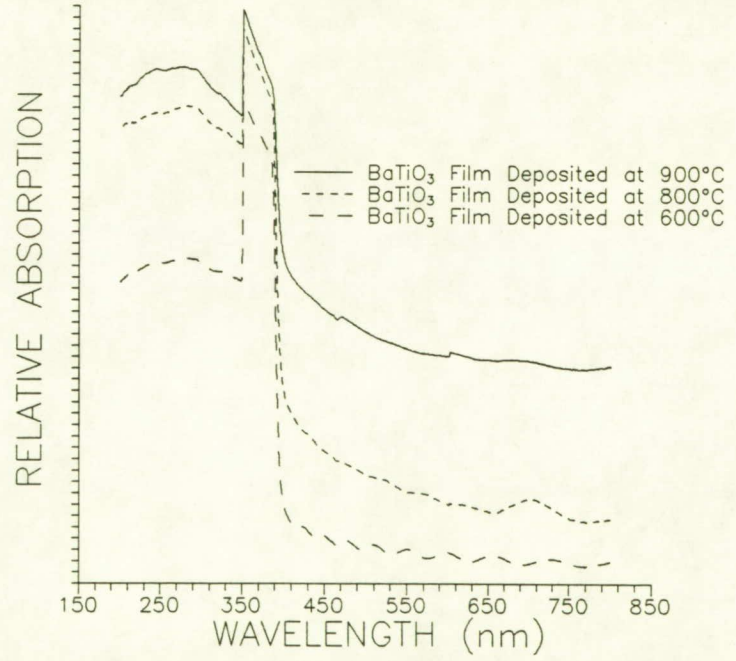

Figure 32. Comparison of UV-Vis spectrometer data from three $BaTiO_3$ films deposited on $SrTiO_3$ at three different deposition temperatures. The absorption tail seen on the higher temperature samples is a characteristic of $BaTiO_3$.

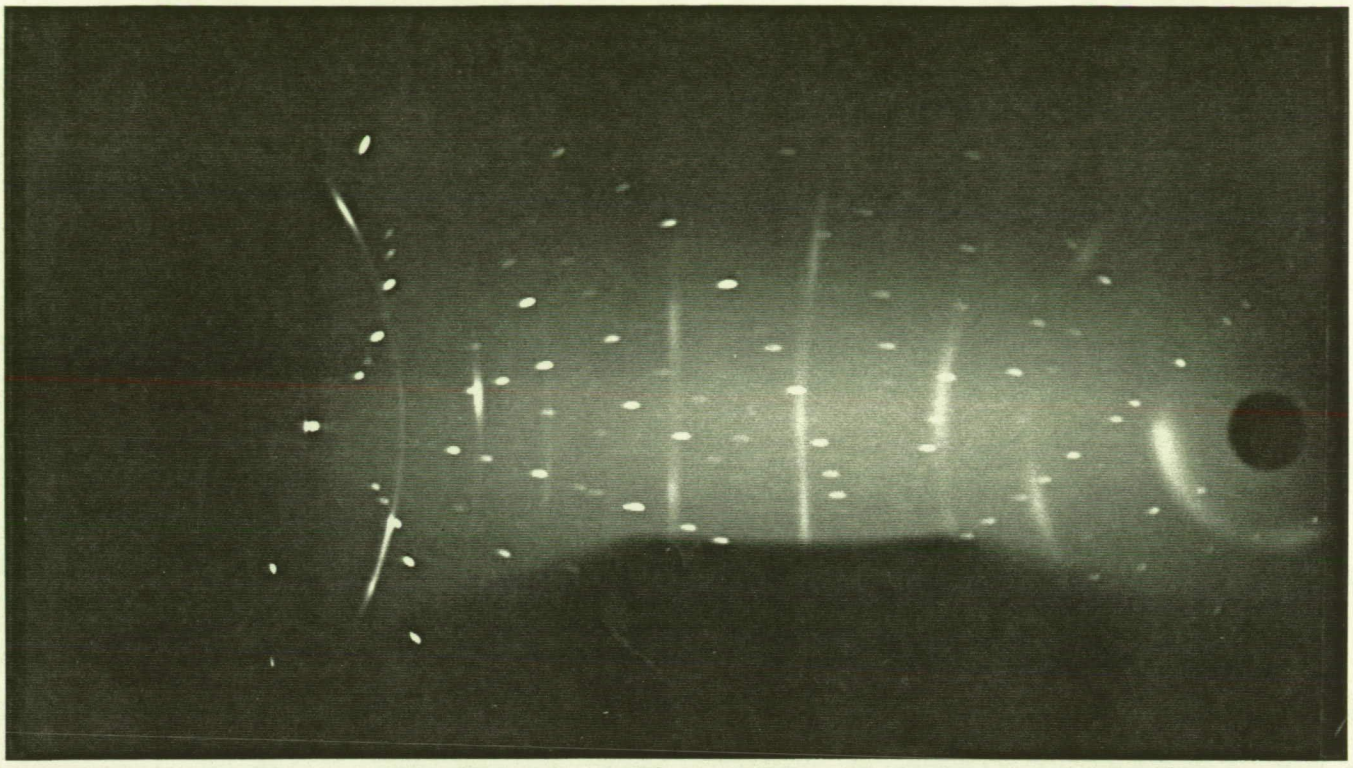

Figure 33. X-ray diffraction pattern from a $BaTiO_3$ film deposited on a 0.5 mm thick $SrTiO_3$ substrate at 900°C exhibits very strong preferential orientation, as indicated by the discontinuous polycrystalline powder lines.

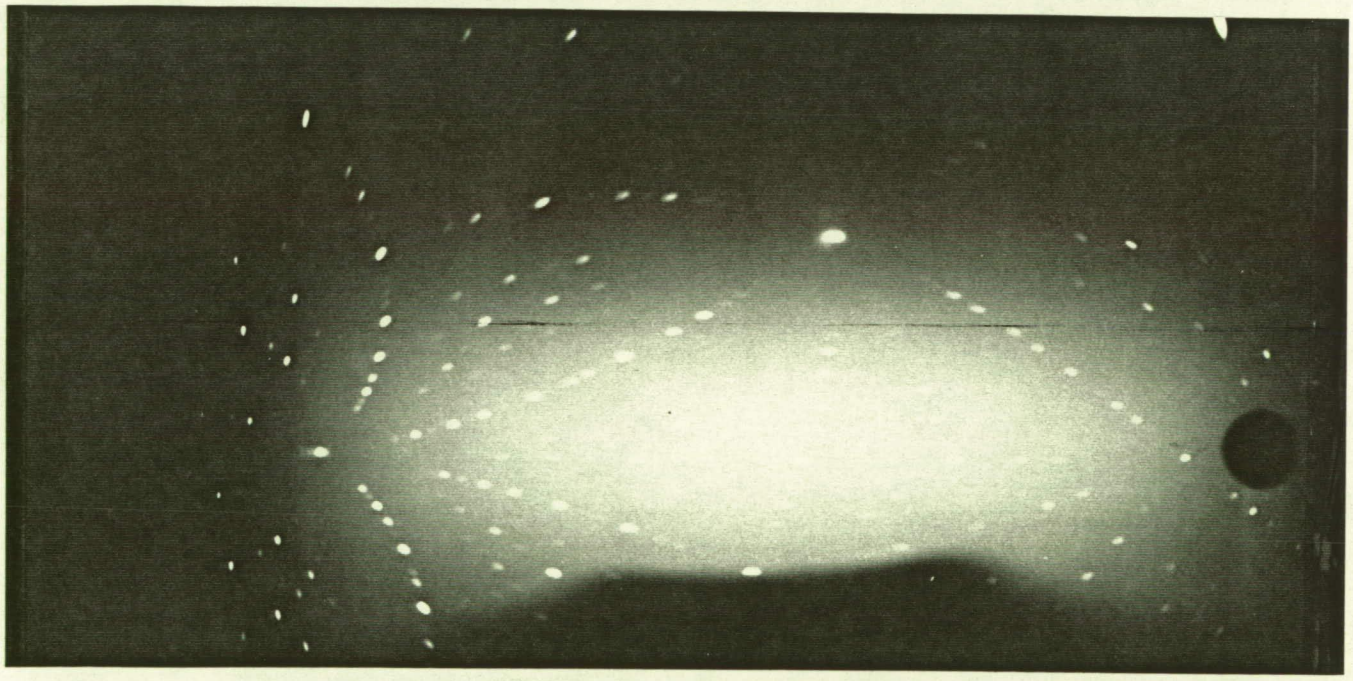

Figure 34. X-ray diffraction pattern from a $BaTiO_3$ film on $SrTiO_3$ indicates no improvement in the crystallinity of the film when using an in situ annealing process.

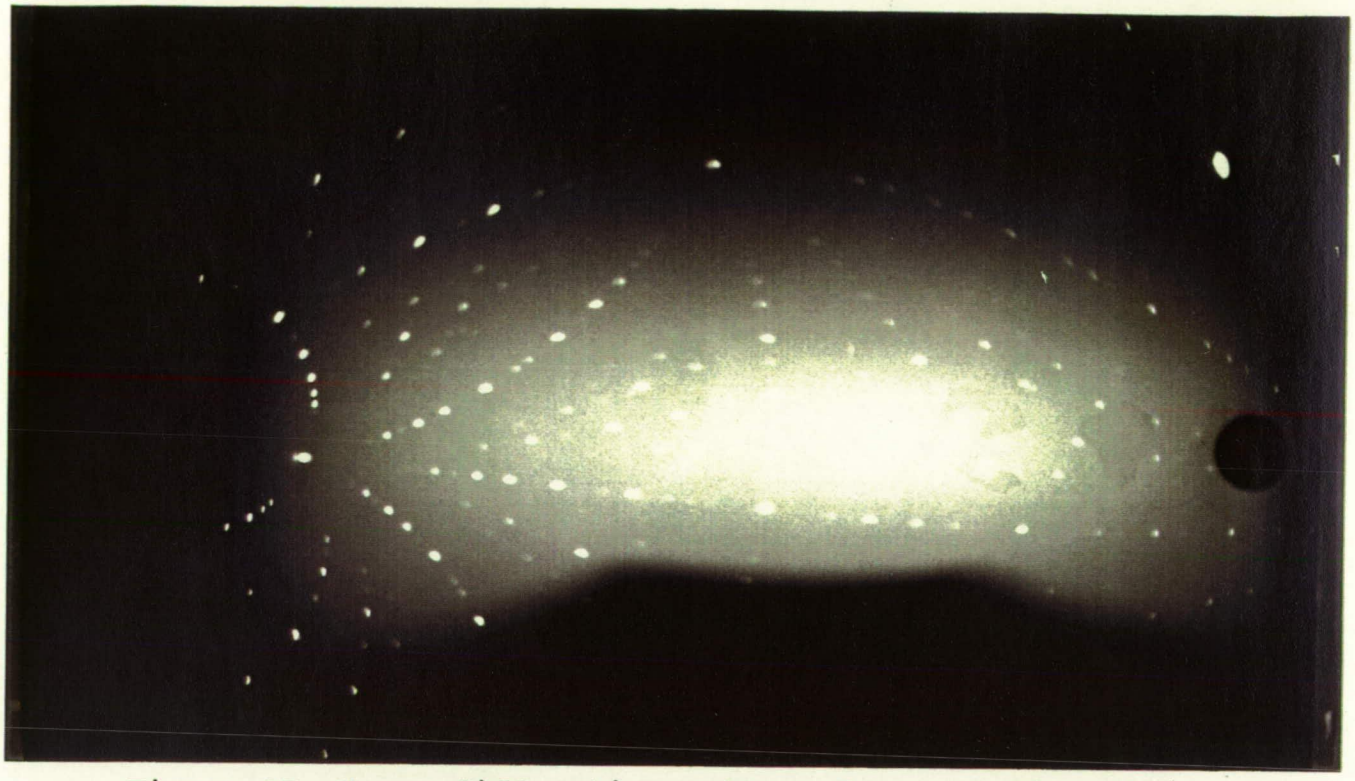

Figure 35. X-ray diffraction pattern from a $BaTiO_3$ film deposited on a 1 mm thick $SrTiO_3$ substrate at 1045°C exhibits slight indications of heteroepitaxial growth.

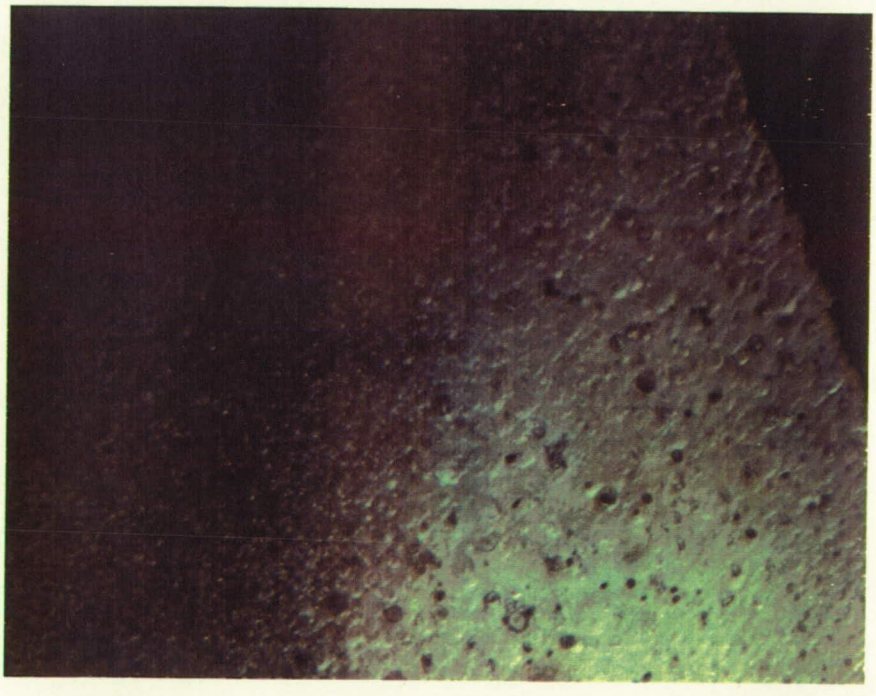

Figure 36. Photomicrograph of a $BaTiO_3$ film on $SrTiO_3$ shows film growth on the surface of the substrate where the conductive paste exists on the back.

Figure 37. X-ray diffraction pattern from a $BaTiO_3$ film deposited on a 1 mm thick $SrTiO_3$ substrate at 1045°C exhibits indications of heteroepitaxial growth and also large grains with texture.

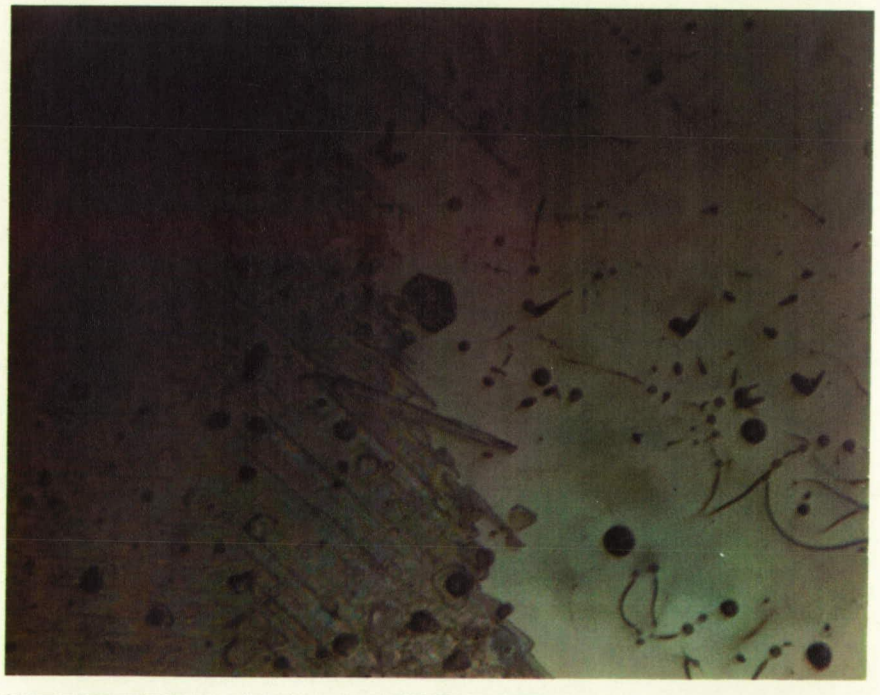

Figure 38. Photomicrograph of a $BaTiO_3$ film deposited on 0.5 mm thick $SrTiO_3$ at 1050°C shows the formation of both the film and a background matrix.

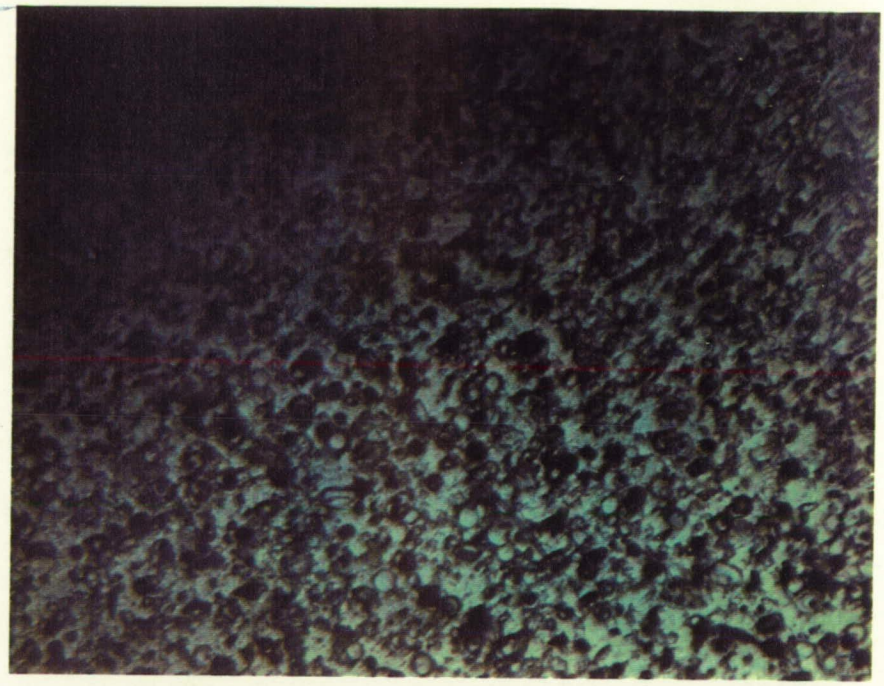

Figure 39. Photomicrograph of the $BaTiO_3$ film on $SrTiO_3$ at about 100x magnification reveals large and symmetrical grains.

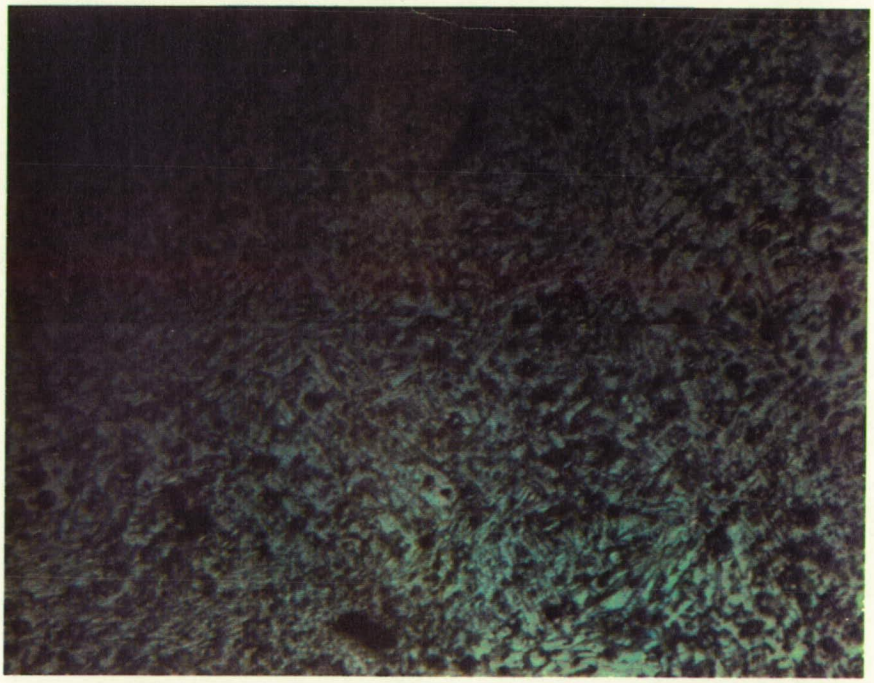

Figure 40. Photomicrograph of the $BaTiO_3$ film on $SrTiO_3$ shows variations in the shape and size of the grains at different locations within the film.

Figure 41. X-ray diffraction pattern from the $BaTiO_3$ film on $SrTiO_3$ shows distorted pairs of diffraction spots, indicating heteroepitaxy, with some faint indications of polycrystallinity.

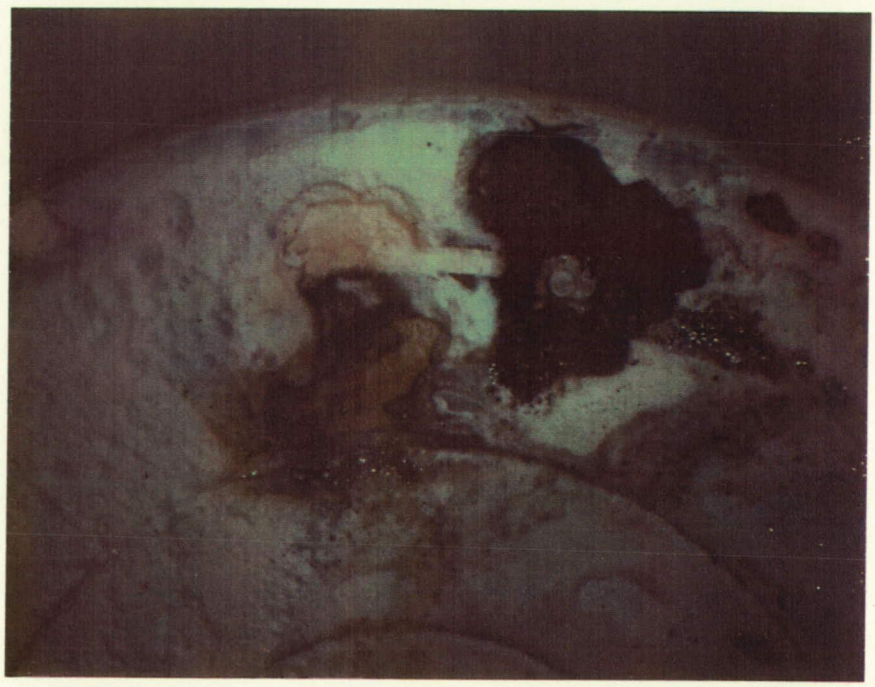

Figure 42. Photomicrograph of the boron nitride coated pyrolytic graphite resistance heater after catastrophic failure (element destroyed - no continuity).

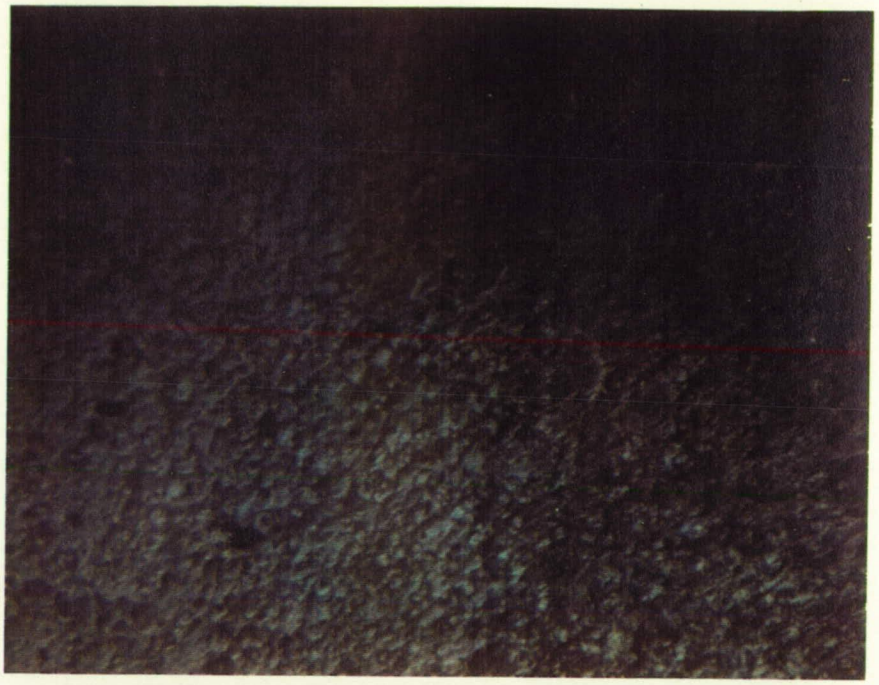

Figure 43. Photomicrograph of the $BaTiO_3$ film on $SrTiO_3$ shows a dark film with small grains resulting from the rapid cool after the heater failure.

Figure 44. Photomicrograph of a section of the $BaTiO_3$ film exposed by the removal of a small piece of the $SrTiO_3$ substrate.

Figure 45. X-ray diffraction pattern from the $BaTiO_3$ film on $SrTiO_3$ exhibits similar but slightly more distorted features in comparison with those seen

Figure 46. X-ray diffraction pattern from a $SrTiO_3$ substrate run through the complete deposition process (temperature cycling) without actually depositing a film.

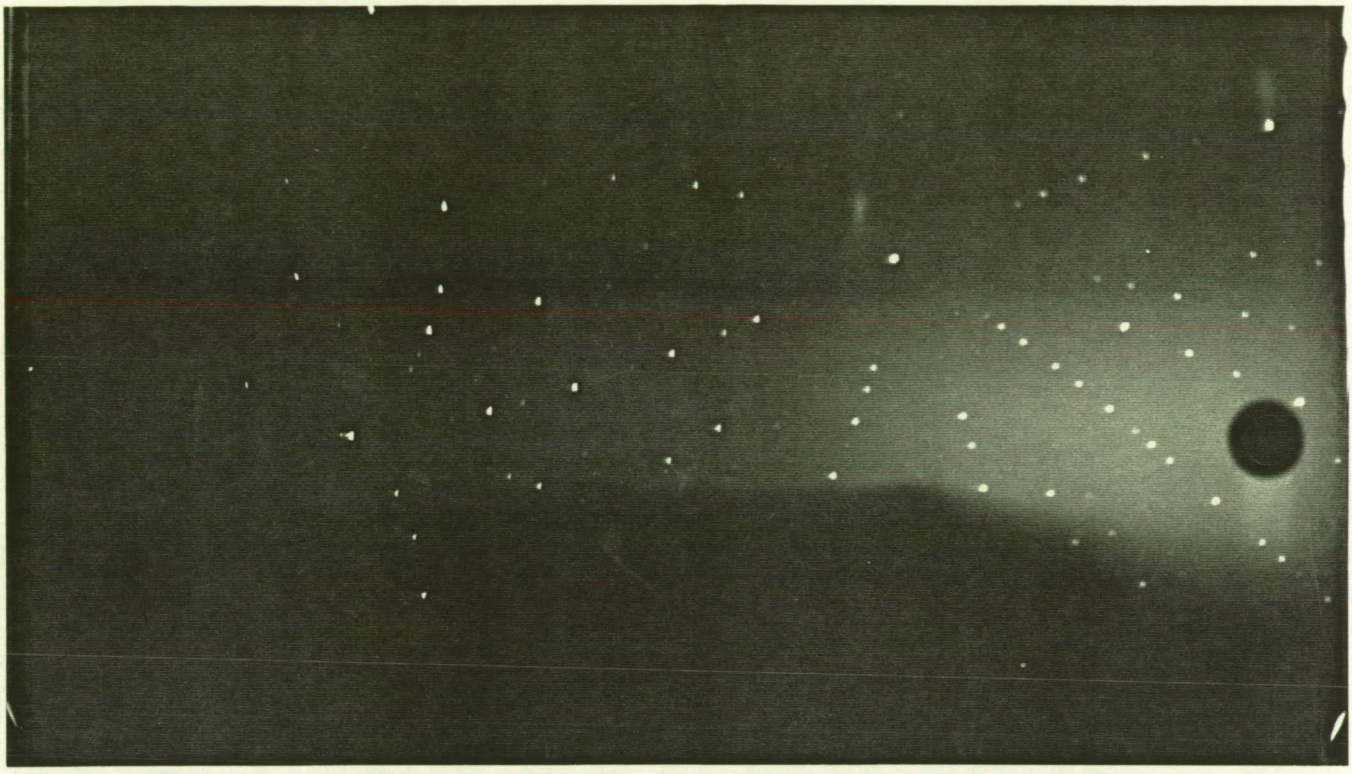

Figure 47. X-ray diffraction pattern from an "off the shelf" $SrTiO_3$ substrate shows inconsistency in the quality of the substrates as produced by the manufacterer.

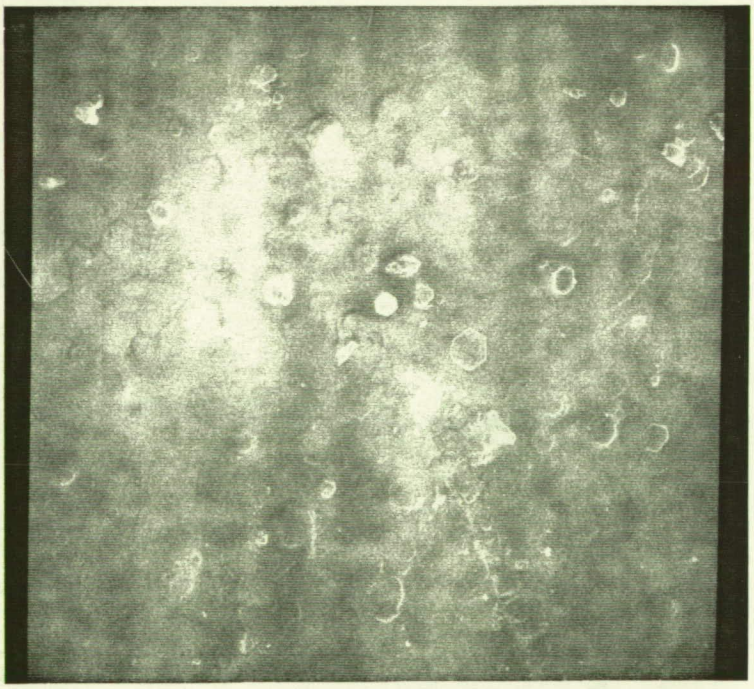

Figure 48. SEM photomicrograph at 200x magnification displays $BaTiO_3$ grains with a hexagonal shape.

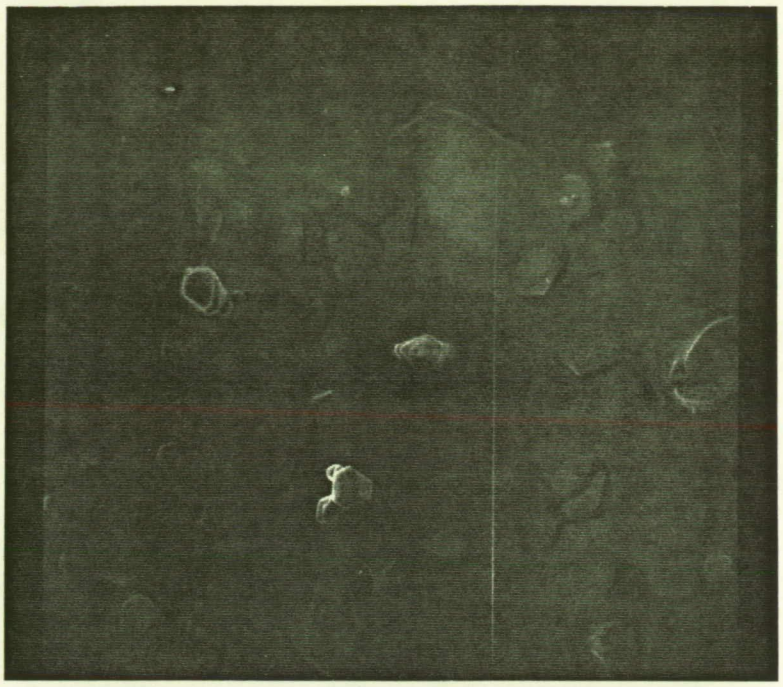

Figure 49. SEM photomicrograph at 200x magnification displays hexagonal $BaTiO_3$ grains, many grains seem to be growing from out of the background matrix material.

Figure 50. SEM photomicrograph at 5000x magnification displays a $BaTiO_3$ grain, 5 to 10 microns on an edge, with a very symmetrical hexagonal shape.

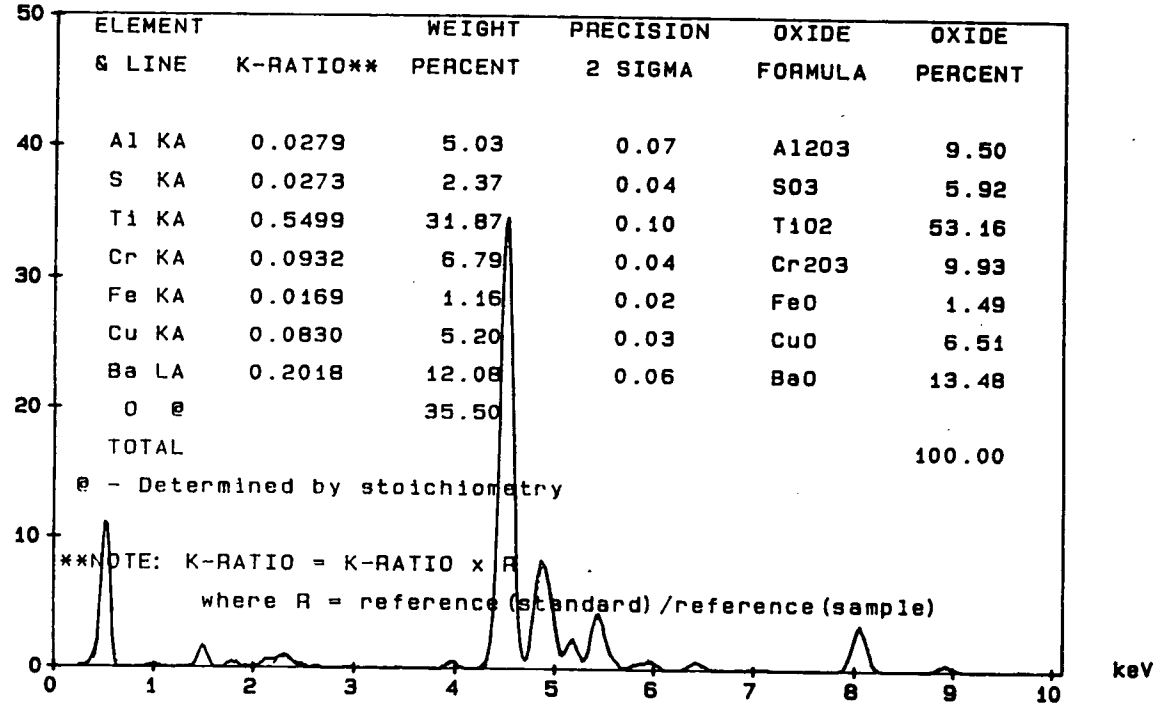

Figure 51. Characteristic x-ray lines and the percentage of various oxides identified using the x-ray compositional analysis does verify the existence of barium, titanium, and oxygen in this film.

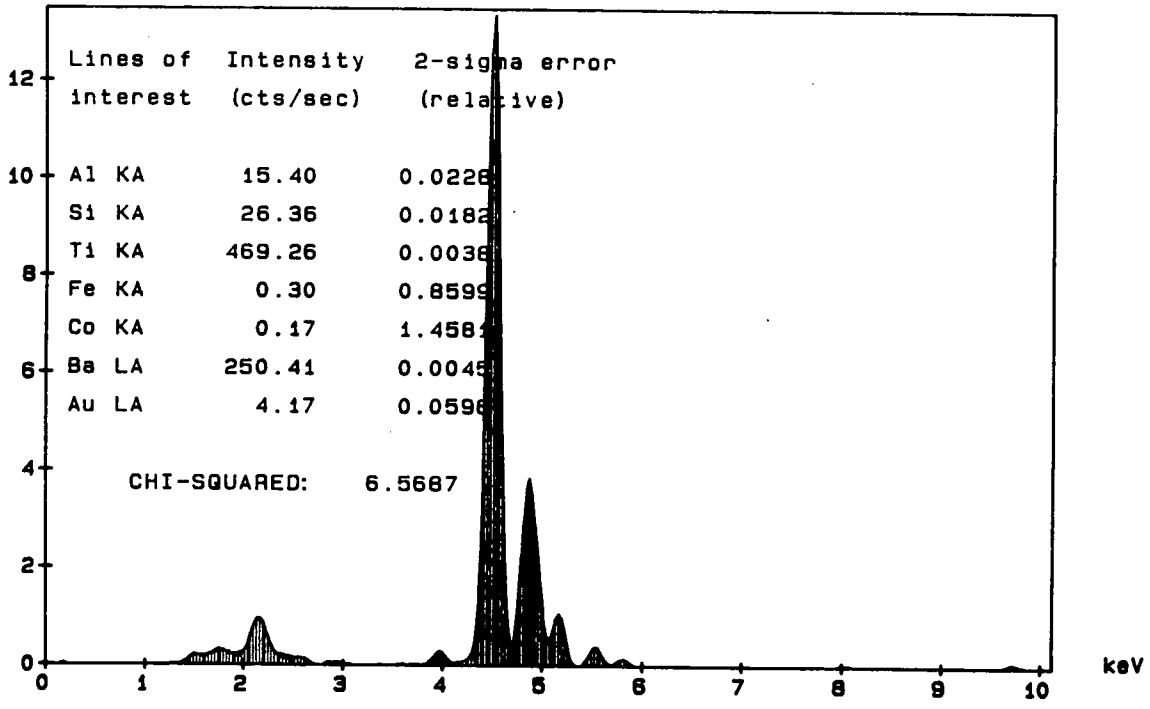

Figure 52. Characteristic x-ray lines and the percentage of various oxides are identified in the x-ray compositional analysis of the standard reference $BaTiO_3$ crystal.

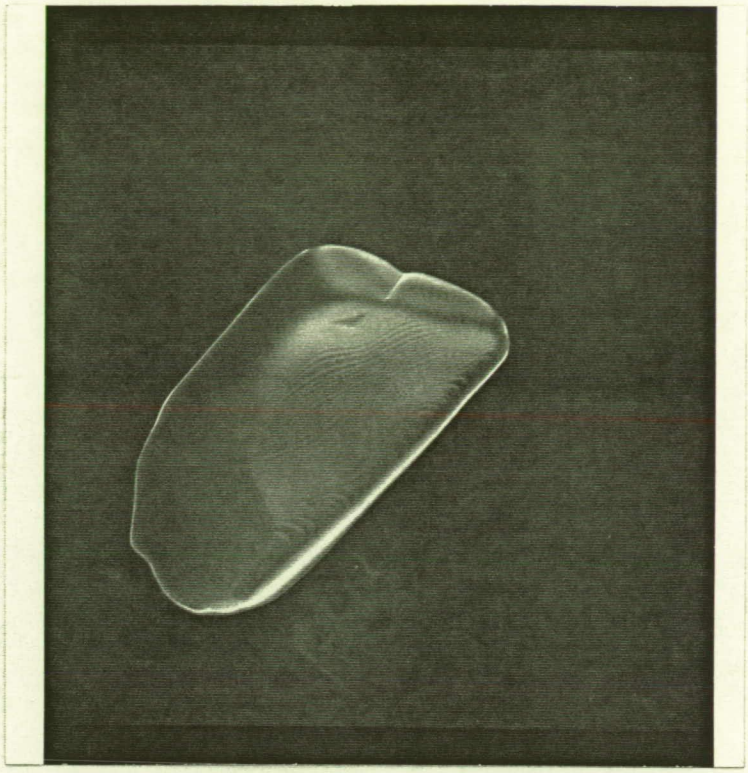

Figure 53. SEM photomicrograph of a $BaTiO_3$ grain at 2000x magnification after the annealing process shows a transformation from the hexagonal shape to a tetragonal shape.

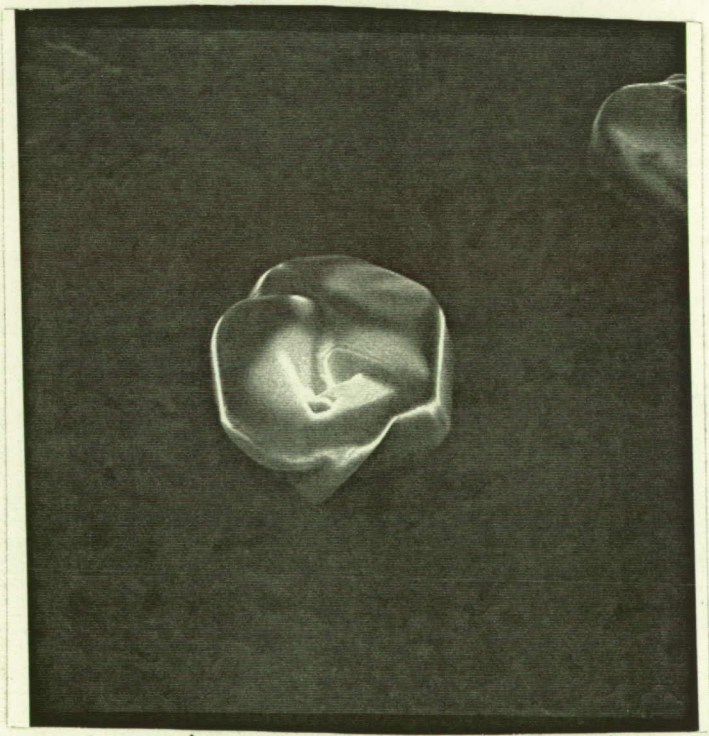

Figure 54. SEM photomicrograph at 2000x manification indicates the collapse of the hexagonal structure in a $BaTiO_3$ grain and the transformation into a tetragonal shape, as a result of annealing.

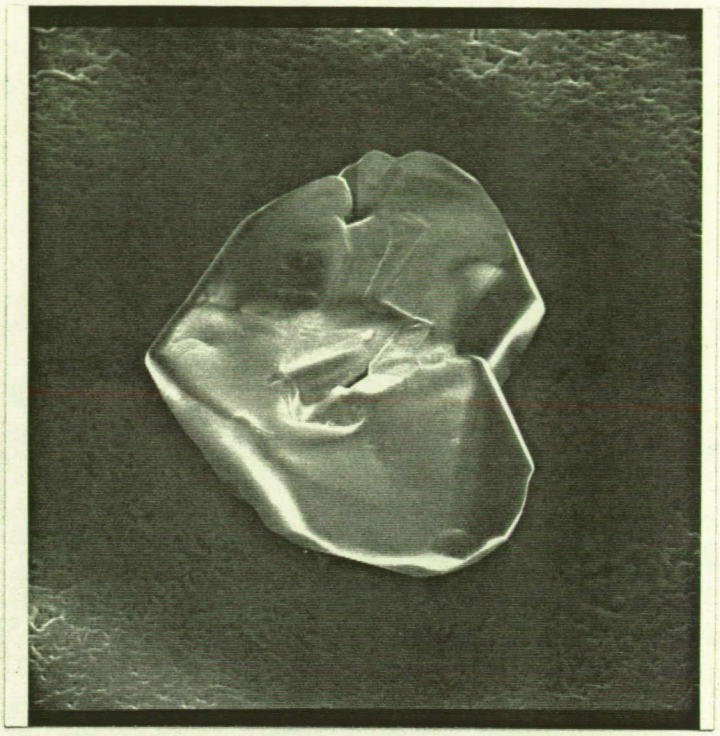

Figure 55. SEM photomicrograph at 1000x magnification shows a $BaTiO_3$ grain which appears to have undergone only partial transformation as a result of the annealing process.

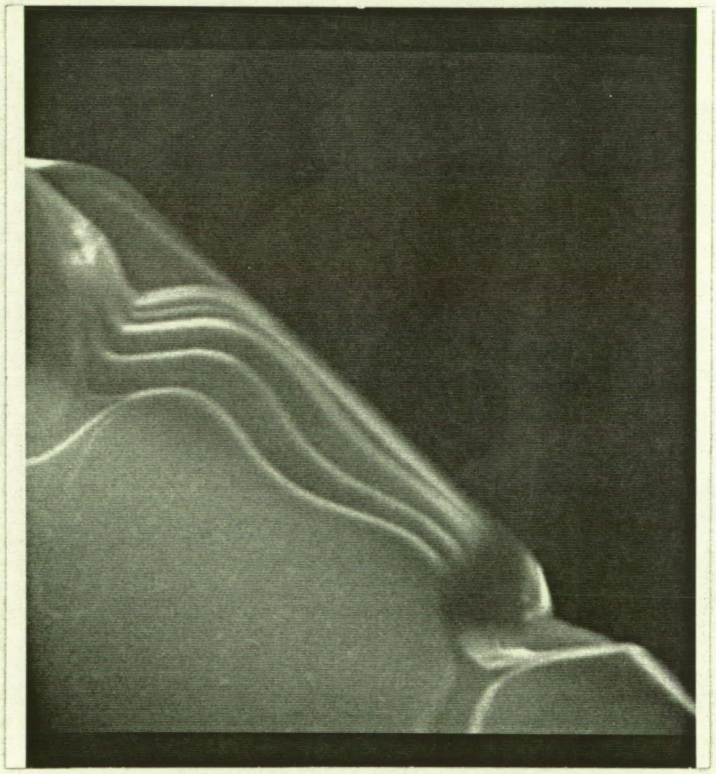

Figure 56. SEM photomicrograph at 10,000x magnification shows the planar stacking within a tetragonal $BaTiO_3$ grain.

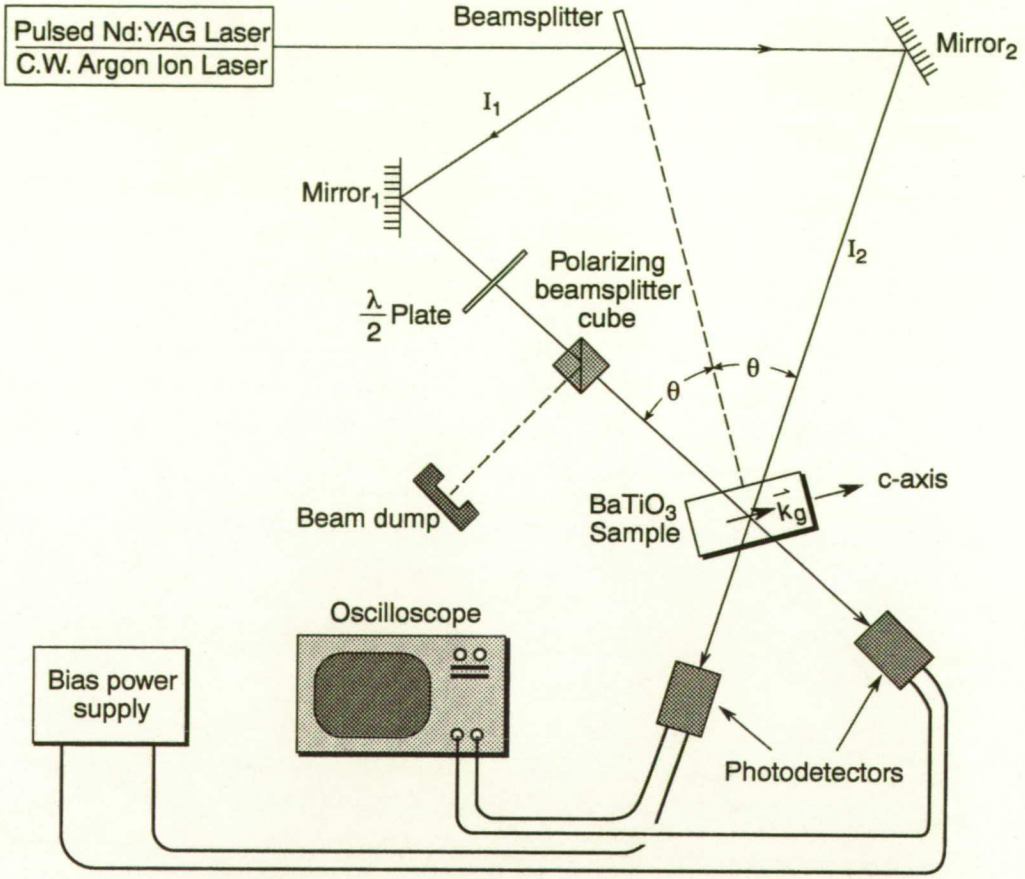

Figure 57. Schematic drawing of the experimental configuration for evaluating two-beam coupling efficiency within $BaTiO_3$ samples.

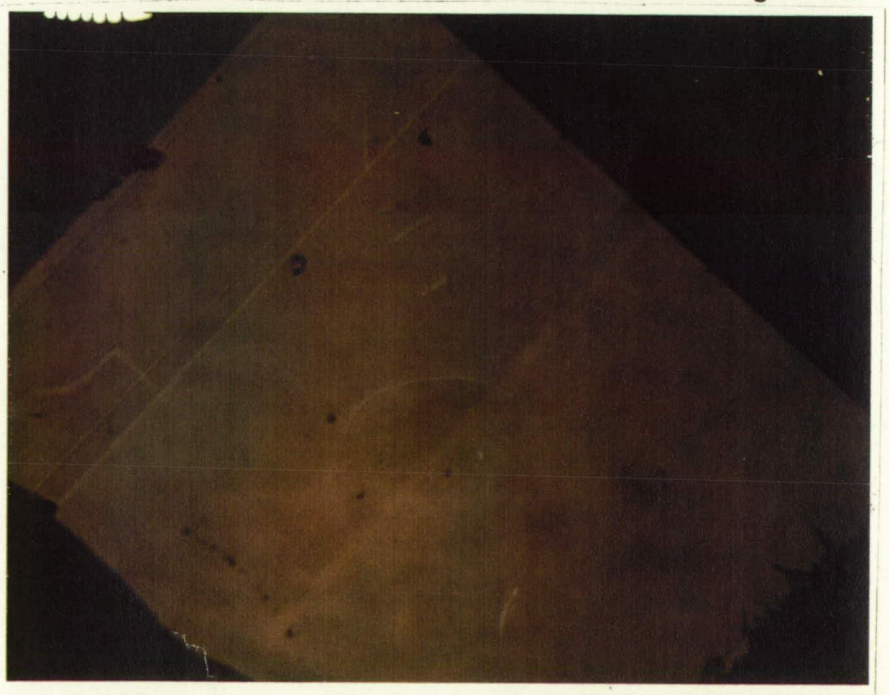

Figure 58. Photomicrograph of a $BaTiO_3$ single crystal sample being examined under normal lighting conditions.

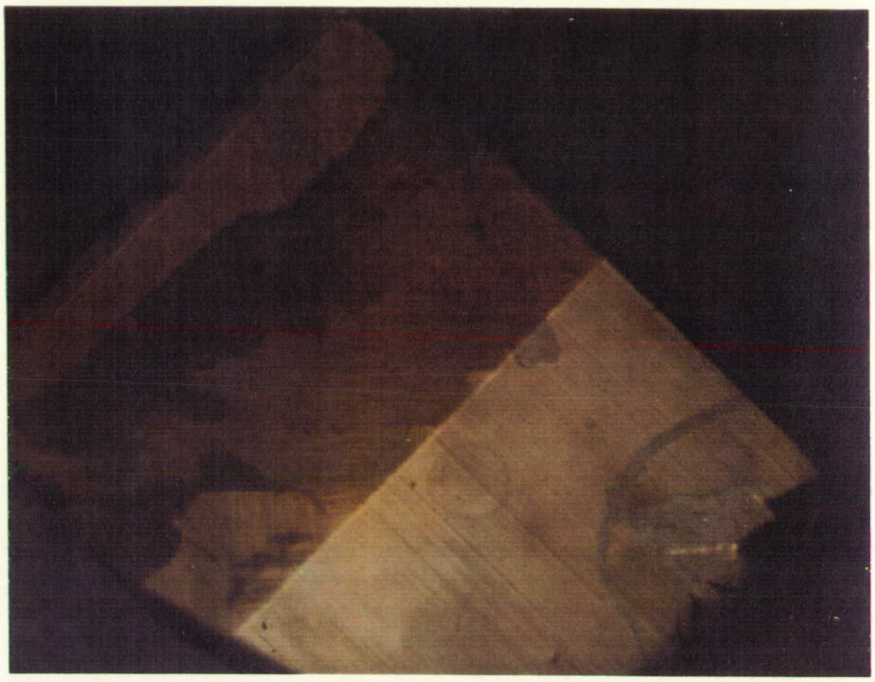

Figure 59. Photomicrograph of the $BaTiO_3$ single crystal sample being examined using polarized light.

Figure 60. Photomicrograph, using polarized light, of the $BaTiO_3$ single crystal sample after interaction with the applied e-field.

Table I. Procedures and Deposition Parameters for Representative Films Deposited by Pulsed Laser Deposition

Substrate	Laser Rep. Rate	Energy per Pulse	Heating Schedule	Temp.	Deposition O_2 Pressure (Flowing)	Time	Cooling Rate/ O_2 Pressure
LiF	10 Hz	100 mJ	250°C - 630°C at 1°C/min	630°C	400 mT	1 hour	1°C/min to 250°C 400 mT
LiF	10 Hz	85 mJ	250°C - 650°C at 1°C/min	650°C	400 mT	2 hours	1°C/min to 250°C 400 mT
LiF	10 Hz	100 mJ	250°C - 650°C at 1°C/min	650°C	0 mT	2 hours	1°C/min to 250°C 200 mT
LiF	5 Hz-5 min 10 Hz-1 hr + 55 min	90 mJ	250°C - 690°C at 1°C/min	690°C	20 mT	2 hours	1°C/min to 250°C 400 mT
LiF	10 Hz	85 mJ	250°C - 690°C at 1°C/min	690°C	22 mT	2.5 hours	55°C intervals at 1°C/min-hold 1 hr repeat down to 250°C - 22 mT
$LaAl0_3$	5 Hz-0.5 hr 10 Hz-1.5 hr	80 mJ	Room temp. to 810°C at 30°C/min	810°C	100 mT	2 hours	Annealed 2 hrs at 825°C-1 atm O_2 1°C/min to 250°C
MgO	5 Hz-1 hr 10 Hz-1 hr	92 mJ	Room temp. to 788°C at 30°C/min	788°C	40 mT	2 hours	0.5 amp/30 min. (≈ 1.25°C/min) 400 mT
MgO	1 Hz-0.25 hr 5 Hz-0.5 hr 10 Hz- 1 hr + 25 min 5 Hz-last 5 min	85 mJ	Room temp. to 820°C at 30°C/min	820°C	100 mT	2.25 hours	Annealed 2 hrs at 825°C-1 atm O_2 1°C/min to 250°C

Table I. Procedures and Deposition Parameters for Representative Films Deposited by Pulsed Laser Deposition (Cont.)

Substrate	Laser Rep. Rate	Energy per Pulse	Heating Schedule	Temp.	Deposition O_2 Pressure (Flowing)	Time	Cooling Rate/ O_2 Pressure
$SrTiO_3$	10 Hz	90 mJ	Room temp. to 600°C at 30°C/min	600°C	400 mT	2 hours	25°C/min 400 mT
$SrTiO_3$	10 Hz	80 mJ	Room temp. to 800°C at 30°C/min	800°C	400 mT	2 hours	25°C/min 400 mT
$SrTiO_3$	10 Hz	90 mJ	Room temp. to 900°C at 30°C/min	900°C	400 mT	1.75 hours	25°C/min 400 mT
$SrTiO_3$ (0.5 mm)	10 Hz	110 mJ	Room temp. to 900°C at 30°C/min	900°C	400 mT	1 hour	40°C/min 400 mT
$SrTiO_3$	5 Hz	90 mJ	Room temp. to 790°C at 30°C/min	790°C	400 mT	2 hours	Annealed 1 hr at 825°C-1 atm O_2 5°C/min to 250°C
$SrTiO_3$	5 Hz	95 mJ	Room temp. to 1045°C at 30°C/min	1045°C	40 mT	2 hours	5°C/min to 250°C 40 mT
$SrTiO_3$	5 Hz	100 mJ	Room temp. to 1045°C at 30°C/min	1045°C	400 mT	2 hours	5°C/min to 250°C 400 mT
$SrTiO_3$ (0.5 mm)	5 Hz	85 mJ	Room temp. to 1050°C at 30°C/min	1050°C	400 mT	2 hours	4°C/min to 250°C 400 mT
$SrTiO_3$ (0.5 mm)	5 Hz	90 mJ	Room temp. to 1050°C at 30°C/min	1050°C	400 mT	1 hour & 50 min	30°C/min to 250°C 400 mT